Journal of Alloys and Compounds

Investigation of Electronic, Optical and Thermoelectric Properties of Perovskite BaTMO3 (TM=Zr, Hf): First Principles Calculations

--Manuscript Draft--

Manuscript Number:	JALCOM-D-20-14331R2
Article Type:	Full Length Article
Keywords:	Perovskite; DFT; TB-mBJ; optical; ferroelectric; Thermoelectric
Corresponding Author:	Said Al Azar, Ph.D Ontario Academy JORDAN
First Author:	Said Al Azar, Ph.D
Order of Authors:	Said Al Azar, Ph.D
	Ibrahim Al-Zoubi
	Ahmad A Mousa, PhD
	Riad S Masharfe, PhD
	Emad K. Jaradat, PhD
Abstract:	The structural, electronic, optical, and thermoelectric characteristics of crystalline oxides-perovskites BaTMO3 (TM=Zr or Hf) were investigated using the all-electron full-potential linearized augmented plane wave (FP-LAPW) method within the framework of density functional theory (DFT). The generalized gradient approximation as parameterized in Perdew, Burke, and Ernzerhof (PBE-GGA) was employed to calculate exchange-correlation potential. Also, the modified Becke Johnson exchange potential approximation as parameterized by Tarn and Blaha (TB-mBJ) was used to improve the bandgap estimation. According to our calculations, both perovskites BaZrO3 and BaHfO3 show insulator behavior and have widely indirect band-gap energy (R-Γ) 4.42 (3.39) eV for BaZrO3 and 5.25 (3.69) eV for BaHfO3 from both approaches, TB-mBJ (PBE-GGA), respectively. The optical properties such as dielectric tensor, the refractive index, the absorption coefficient, and the electron loss function have been calculated and analyzed. The optical transitions mainly take place if an electron radiate from the initial state O-2p to the final state Hf-5d or to the Zr-4d in BaHfO3 or BaZrO3 case, respectively. Furthermore, the transport characteristics calculations based on semi-classical Boltzmann theory have been discussed. The thermopower at RT of both compounds BaHfO3 and BaZrO3 are 260.47 and 208.33 μV/K, respectively. This result is good enough to consider these materials as promise thermoelectric candidates. Our results were compared with the previous ab intio calculations and experiments and showed a reasonable agreement.
Order of Authors (with Contributor Roles):	Said Al Azar, Ph.D
	Ibrahim Al-Zoubi
	Ahmad A Mousa, PhD
	Riad S Masharfe, PhD
	Emad K. Jaradat, PhD

Cover Letter

Said M. Al Azar

Ontario Academy

Amman 11512, Jordan

Phone:+962786767222

Date: 8 November 2020

Dear Ludwig Schultz Editor –in-Chief of Journal of Alloys and Compounds,

I am pleased to submit an original research article entitled " Investigate of Electronic, Optical and Thermoelectric Properties of Perovskite $BaTMO_3$ (TM=Zr, Hf): First Principles Calculations" by Said Al Azar, Ibrahim Al-Zoubi, Ahmad Mousa Riad Masharfe, and Emad K. Jaradat for consideration for publication in Journal of Alloys and Compounds.

In this manuscript, the Tran-Blaha parameterized of the modified Becke-Johnson (TB-mBJ) exchange potential, was used to predict the band gap of two perovskites $BaZrO_3$ and $BaHfO_3$. The results were compared with the standard GGA-DFT calculations. Also, the semiclassical Boltzmann transport theory program (PoltzTrap) was employed to predict the thermoelectric properties of these two perovskites.

We believe that this manuscript is appropriate for publication by Journal of Alloys and Compounds because it is consistent with the aim and scope of this prestigious journal.

Please let me know if you prefer suggesting names of possible reviewers in the field. On behalf of me and all authors, I'd like to thank you for your consideration of this manuscript.

Sincerely,

Dr. Said Al Azar

Professor of Physics and Corresponding author

Prime Novelty Statement

The prime novelty of this research article is to investigate the thermoelectric and optical properties of the Ba(Zr, Hf)O_3 perovskite alloys by using density functional theory (DFT) and semi-classical Boltzmann transport theory. Although the two compounds showed weak thermoelectric characteristics, their physical properties are diverse and easy to tune.

Manuscript JALCOM-D-20-14331

Response to Reviewers

Dear editor,

Thank you for giving us the opportunity to submit a revised draft of the manuscript "**Investigation of Electronic, Optical and Thermoelectric Properties of Perovskite BaTMO3 (TM=Zr, Hf): First Principles Calculations**" for publication in the Journal of Alloys and Compounds. We appreciate the time and effort that you and the reviewers dedicated to providing feedback on our manuscript and are grateful for the insightful comments on and valuable improvements to our paper. We revised our manuscript and, the required amendments for scientific and non-scientific issues were performed. Furthermore, some issues should be explained and discussed here.

First of all, we did an intensive revise and refinement of the English language. Also, the format of the article, such as the paragraph alignment and references, is modified. The number of figures was reduced by reorganized some them into one figure and labeled a), b), etc.

Response of reviewers:

About the comments of reviewer #1

Thank you for your valuable comments. We amended the abstract and discussed in more detail the results especially thermoelectric properties. We do all the scientific and non-scientific issues (Updated text in the manuscript is highlighted).

About the comments of reviewer #4

We thank reviewer #4 for your valuable comments. We performed all suggested comments in the revised manuscript (Updated text in the manuscript is highlighted).

About the first comment of reviewer #4 we added a detail discussion as it appear in the updated text.

Also, for the second and third comments, detail discussions are added to the text.

And about the single crystal some details are added to the introduction.

We thank reviewer#5 for your comments and we amended the manuscript (Updated text and figures in the manuscript). Also, the number of references was reduced.

About the fourth comment of reviewer #5,

Although their thermoelectric properties seem not good as expected, their promise potential is still found, and there is a probability to improve their properties by nanoengineering or doping. Also, this is the first time to study its transport properties in detail according to our knowledge. Furthermore, our results contradict a recently published study about $BaHfO_3$ [Eur. Phys. J. B (2020) 93: 218]. It strongly supports that $BaHfO_3$ is one potential candidate in thermoelectric applications.

Also, about the fifth comment of reviewer #5

Reviewer asked about the temperature ranges of figures 13(a), 14(a), 15(a), and 16(left). As you see, all figures have a temperature range but not all panels in the same figure because all panels have the same temperature range, so we did not repeat the range in each panel.

About the comments of reviewer #6

According to our knowledge, there are many computational studies in physics and materials science carried out without the experimental aspects, or there was a lack of experimental data. These studies contributed to new discoveries in the field. Also, sometimes their results could be more precise than experiments. We tried to support our results with available experimental data. This opinion does not affect our work and results. Furthermore, we discussed in more detail the underlying mechanisms related to our results.

We would like to **thank the referee again** for taking the time to review our manuscript.

Sincerely,

The authors of paper

Investigation of Electronic, Optical and Thermoelectric Properties of Perovskite $BaTMO_3$ (TM=Zr, Hf): First Principles Calculations

Said Al Azar[1*], Ibrahim Al-Zoubi[2], Ahmad Mousa[3], Riad Masharfe[4], Emad K. Jaradat[2]
[1] Research and Development Department, Ontario Academy, Amman, Jordan
[2] Department of Physics, Mutah University, Karak, Jordan.
[3] Department of Basic Sciences, Middle East University, Amman, 11831, Jordan
[4] Physics Department, Zarqa University, Zarqa, Jordan

Abstract: The structural, electronic, optical and thermoelectric characteristics of crystalline oxides-perovskites $BaTMO_3$ were investigated using all-electrons full-potential linearized augmented plane wave (FP-LAPW) method within the framework of density functional theory (DFT). These calculations are performed using the computer code WIEN2k. The generalized gradient approximation as parameterized in Perdew, Burke and Ernzerhof (PBE-GGA) is employed to calculate exchange-correlation potential. Also, the modified Becke Johnson exchange potential approximation as parameterized by Tarn and Blaha (TB-mBJ) is used to improve the band gap estimation. The comparison among the previous ab intio calculations, the experimental measurements, and our study results are done. In our calculations, it is shown that these two perovskites $BaZrO_3$ and $BaHfO_3$ are insulators and have widely indirect band-gap energy (R-Γ) from both approaches, PBE-GGA and TB-mBJ. The optical properties such as dielectric tensor, the refractive index, the absorption coefficient, and the electron loss function have been calculated and analyzed. Furthermore, the transport characteristics calculations based on semi-classical Boltzmann theory have been discussed.

Keywords: Perovskite, DFT, PBE-GGA, TB-mBJ, Optical, Ferroelectric, $BaZrO_3$, $BaHfO_3$, Thermoelectric.

*corresponding author (Said Al Azar; Email: q_saed74@yahoo.com)

1. Introduction

Both Barium zirconate ($BaZrO_3$) and Barium hafinate ($BaHfO_3$) perovskites get more attention experimentally [1–7]and theoretically [8–13] because of their unique physical properties and potential applications as functional materials. They show an extensive variety and fascinating such as high thermoelectric power, ferroelectricity, piezoelectricity frequency doublers, superconductivity, giant magnetoresistance, and the exchange of structural, optical, magnetic, electronic characteristics [2,14,15]. The Perovskites (ABX_3), A and B are cations and X is an anion, there are many kinds of the perovskite structure crystals, such as the oxides-perovskites (ABO_3), flouro-perovskites (ABF_3), anti-perovskite (A_3BX), double-perovskite (A_2BO_6) and nitrides-anti-perovskites (A_3BN)[16].

Barium zirconate, $BaZrO_3$ is a surface effect ceramic material that has many mechanical and technological applications[17]. Also, $BaZrO_3$ has some unique properties such as high dielectric constant (~50). And it has high thermal stability and wide bandgap energy (~4 eV). These diverse properties have placed this perovskite ceramic as a useful material in applications like microwave devices, and high-temperature proton conductor for electric ceramics [3]. King-Smith and Vanderbilt calculated lattice constants, band structures, zone-center phonon frequencies, and elastic constants using the FLAPW method, with the exchange local density approximation (LDA) [8]. Barium hafnate $BaHfO_3$, is the compound have high-temperature melting (2893K), physical unique properties have been studied in both experimental and theoretical terms including thermal expansion coefficient, heat capacity, thermal conductivity, hardness, by using the X-ray diffraction pattern, and the lattice parameter of 0.4171 nm at room temperature [18]. Also, Vali studied the properties such as the electronic band structure, phonon dispersion and dielectric constants of $BaHfO_3$ using DFT. He found that $BaHfO_3$ has an indirect bandgap between (R-Γ) points about 3.533 eV[19].

Thin films of $BaHf_{1-x}TiO_3$ are deposited using pulsed liquid injection MOCVD technique on Si (100) substrate. The roughness average value (Ra) of the film is increasing with increase x-value. Also the $BaHf_{0.75}Ti_{0.25}O_3$ thin film shows well-behavior capacitance-voltage characteristic and its k-value is around 14 [20]. Evarestov investigated the structure stability for both $BaZrO_3$ and $BaHfO_3$ perovskites using hybrid functional DFT with phonon frequency calculations. The Mulliken and Born atomic charges results are emphasized the stability of cubic and covelant bonds in both crystals [12].

Photoluminescence and photocatalytic activity of bismuth doped $BaZrO_3$ were investigated experimentally using powder X-ray diffraction (XRD), UV–VIS diffuse reflectance spectroscopy, photoluminescence (PL) spectroscopy, and photocatalytic activity. The results suggested that $BaZrO_3$:Bi could be a good candidate to be used as a visible-light activated photocatalyst under excitation wavelengths less than 800 nm [21]. Parida et al synthesized $BaZrO_3$ ceramic powder by the solid state reaction method. Their measurement indicated that $BaZrO_3$ could be used for small dielectric resonator antenna (DRA) technology because of its low less

microwave dielectrics materials [22]. Khan and Qureshi observed that Tantalum doped $BaZrO_3$ at Ta concentration $x = 0.04$ ($BaZr_{0.96}Ta_{0.04}O_3$) gives the highest rate of hydrogen evolution (180μmol/h) along with the surface area [23].

Zhang et al conclude that the spontaneous polarization, Born effective charge and dielectric of $BaZrO_3$ is significantly sensitive to epitaxial strain and the transition from paraelectric to ferroelectric happened in both compressive and tensile strain. $BaZrO_3$ could be useful for tunable dielectric materials [24]. Chen et al synthesis $BaZrO_3$ hollow nanostructure with oxygen vacancies through one step solvothermal method using ethylenediamine (EDA) as solvent for photocatalytic hydrogen evolution from pure water. The H_2 production rate is about 15 times than that of the commercial $BaZrO_3$ (BZO-C) [25]. The $BaZrO_3$ hollow nanocrystal dopant by Fe^{+3} ions were prepared through facile solvothermal method for photocatalytic H_2 from pure water under visible light. The existence of Fe (III) ion plays a key role in broadening the optical absorption range and restricting the recombination of photo-induced carriers under visible light irradiation [8,26,27].

Although these two perovskites are studied intensively, the literature review indicates that there is a paucity of thermoelectric data and calculations. The main goal of this research study is to review and investigate in details the ferroelectric and thermoelectric properties of the cubic Barium Zirconate and Barium Hafnate perovskites to design new potential applications in ferroelectric and thermoelectric technologies.

This contribution is organized as follows: an introduction with the previous overview, the computational and theoretical framework details, the results and discussion with the comparison with previously available data, and finally the conclusions are drawn.

2. Computational Details

We have performed total energy calculations for the oxides-perovskite $BaTMO_3$, an ideal cubic structure that contains only one, composed of four atoms in its unit cell. The cations Ba are at the cube corners, 1a (0, 0, 0), while the cations TM are at the center of the cube, 1b (½, ½, ½) and oxygen atoms at the center of the cube faces forming a regular octahedron, 3c (0, ½, ½) sites of Wyckoff coordinates, as shown in Figure1. The space group for these two perovskites is Pm-3m (#221). We have used the interstitial region to express plane waves are used approximation for the calculation of exchange-correlation energy functional, namely; generalized gradient approximation (GGA) of Perdew, Burke and Ernzerhof (PBE) parameterization [28] and using modified Becke Johnson exchange potential approximation as parameterized by Tran and Blaha (TB-mBJ) to calculate the electronic band structure and density of states [29,30]. The TB-mBJ method was known that it provides more accurate energy band gap values than PBE-GGA method with cheap calculations cost. Where the first-principles calculations were performed based on (DFT) to describe the ground state [31,32]used the method of (FP-LAPW) [33–35] this is

performed using the computer code in Wien2k code [36]. Also, we chose the interstitial area of the plane wave with a cutoff $K_{max} \times R_{MT} = 8$, where R_{MT} is the smallest muffin-tin radius in the unit cell, also K_{max} is the largest K vector magnitude of the interstitial plane-wave expansion of the basis set. The chosen number of k-points is (16×16×16) in codes, and which corresponds to the total number of k-points of 4096.

For the optical properties, we calculated the complex dielectric function $\varepsilon(\omega) = \varepsilon_1(\omega) + i\varepsilon_2(\omega)$, where $\varepsilon_1(\omega)$ is the real part and $\varepsilon_2(\omega)$ is the imaginary part. The real part $\varepsilon_1(\omega)$ of dielectric function $\varepsilon(\omega)$ gives from the Kramer–Kronig relationship:

$$\varepsilon_1(\omega) = 1 + \frac{2}{\pi} P \int_0^{\infty} \frac{\acute{\omega}\varepsilon_2(\acute{\omega})}{(\acute{\omega})^2 - \omega^2} d\acute{\omega} \quad [1]$$

where the P is the principle value of the integral. The imaginary part $\varepsilon_2(\omega)$ was calculated from the momentum matrix elements between the occupied and unoccupied wave functions within the selection rules

$$\varepsilon_2(\omega) = \left(\frac{\hbar^2 e^2}{\pi m^2 \omega^2}\right) \sum_{c,v} \int d^3 k \langle ck|p^{\alpha}|vk\rangle\langle vk|p^{\beta}|ck\rangle \times \delta(\varepsilon ck - \varepsilon vk - \omega) \quad [2]$$

where p is the momentum matrix element between states of bands α and β with crystal momentum k. c_k and v_k are the crystal wave functions corresponding to the conduction, and valance bands with crystal wave vector k [37]. There are two contributions to ε(ω), namely; inter-band and intra-band transitions. The contribution inter-band is important only for metals, where be inter-band between valence-to-conduction absorption spectra. Whereas intra-band between valence-to-valence and conduction-to-conduction absorption. Which is describes the complete response of a material to the applied electromagnetic radiations field [38]. Then, the main optical parameters: the refractive index $n^{ii}(\omega)$, the extinction coefficient $k^{ii}(\omega)$, the absorption coefficient $\alpha^{ii}(\omega)$, optical conductivity $\sigma^{ij}(\omega)$, electron loss energy function $L^{ij}(\omega)$, and the normal incidence reflectivity $R^{ii}(\omega)$ in the crystal are given by [39,40].

$$n^{ii}(\omega) = \left[\frac{\sqrt{\varepsilon_1^{ii2}(\omega) + \varepsilon_2^{ii2}(\omega)} + \varepsilon_1^{ii}(\omega)}{2}\right]^{1/2} \quad [3]$$

$$k^{ii}(\omega) = \left[\frac{\sqrt{\varepsilon_1^{ii2}(\omega) + \varepsilon_2^{ii2}(\omega)} - \varepsilon_1^{ii}(\omega)}{2}\right]^{1/2} \quad [4]$$

$$\alpha^{ii}(\omega) = \frac{2\omega k^{ii}}{c} \quad [5]$$

$$Re\sigma^{ij}(\omega) = \frac{\omega}{4\pi} Im\varepsilon_{ij} \quad [6]$$

$$L^{ij}(\omega) = \sqrt{2}\omega\left[\sqrt{\varepsilon_1^{ij2}(\omega) + \varepsilon_2^{ij2}(\omega)} - \varepsilon_1^{ij}(\omega)\right]^{½} \quad [7]$$

$$R^{ii}(\omega) = \frac{n^{ii}+ik^{ii}-1}{n^{ii}+ik^{ii}+1} \quad [8]$$

The transport properties are obtained from the analysis of band structure results based on Boltzmann theory method under the relaxation time approximation as implemented in BoltzTraP code [41,42]. To explore the properties of thermoelectric such as Seebeck coefficient (S), electrical conductivity (σ), specific heat (C_e), electronic thermal conductivity (κ°), and power factor rate (PF). A dense k-mesh of 25000 in the full Brillouin zone was used to guarantee good results.

The Seebeck coefficient (S) is related to carrier concentration via the Mott formula as follows [43]:

$$S = \frac{\pi^2 k_B T}{3e}\left\{\frac{1}{h}\frac{dn(E)}{dE} + \frac{1}{\mu}\frac{d\mu(E)}{dE}\right\} \quad [9]$$

where *e* is the electron charge, k_B is Boltzmann constant, *h* is the Planck constant, μ is carrier mobility and *n* is the carrier concentration.

Electrical conductivity (σ) is related to carrier concentration as follows[44]:

$$\sigma = \frac{ne^2\tau}{m} \quad [10]$$

where *m* is the electron mass, *n* is the carrier concentration and τ is the relaxation time.

Electronic specific heat (C_e) is related to temperature and chemical potential as follows [45]:

$$C_e(T;\ \mu) = \int n(\varepsilon)(\varepsilon-\mu)\left[\frac{df\mu(T;\varepsilon)}{dT}\right]d\varepsilon \quad [11]$$

3. **Results and Discussion**

3.1 **Structural Properties**

Goldschmidt tolerance factor (t) for perovskite is given by[46]:

$$t = \frac{(r_A+r_X)}{\sqrt{2}(r_B+r_X)} \quad [12]$$

Where $r_N$is the ionic radius of atom N. The t values of existence perovskite compounds range is ($0.75 < t \leq 1$). For ideal cubic perovskite structure, t has unity value. The tolerance factor t for $BaZrO_3$ and $BaHfO_3$ are 1.0 and 1.016, respectively.

We presented the relationship between the energy changes as a function of the unit cell volume. Using the Birch-Murnaghan equation of state to determine the different important structural and ground-state properties [47]. The equilibrium lattice constants (α) and ground-state energies (E_0) are calculated, as estimated from optimization at zero pressure. Besides the volume,

the lattice constants increase because of the increase in the atomic radius from Zr to Hf. In the present work, we were fitting the energy-volume values to a third-order Birch Murnaghan equation of state to calculate lattice parameter α and bulk modulus B_0 of Ba(Zr, Hf)O_3 compounds, where the bulk modulus increases as the volume decreasing with moving of cation down in the group in the periodic table. The calculated ground-state parameters for both $BaZrO_3$ and $BaHfO_3$ are tabulated in Table 1 along with previous computational and experimental studies. For both perovskites, our results are in reasonable agreement with the available experimental data and previous calculations.

3.2 Electronic properties

To study the electronic properties of $BaZrO_3$ and $BaHfO_3$, DOS's and band structures along the symmetry direction of the first Brillouin zone, of these compounds both PBE-GGA, and TB-mBJ methods for exchange-correlation potential are used. The band structures for $BaZrO_3$ and $BaHfO_3$ are presented in figures 2 and 3 respectively. The Fermi level E_F is chosen to locate at 0 eV. In both methods, the $BaZrO_3$ shows semiconductor characteristics with indirect bandgap (E_g) ($R \rightarrow \Gamma$), but in the TB-mBJ method, the (E_g) is wider. The valence band maximum (VBM) occurs along the R-point symmetry line, while the conduction band minimum (CBM) occurs along the Γ-point symmetry line. The bandgap approaches 3.39 eV by using the PBE-GGA method whereas it approaches 4.424 eV by using the TB-mBJ method. As well, $BaHfO_3$ shows the same behavior with indirect semiconductor bandgap ($R \rightarrow \Gamma$), where the bandgap is 3.69 eV by using the PBE-GGA method and 5.246 eV when using the TB-mBJ method. Table 2, the calculated bandgap (E_g) of both perovskites $BaZrO_3$ and $BaHfO_3$ are compared with previous theoretical and experimental data. For both compounds, the TB-mBJ values approach more enough to experimental results.

The total density of state (TDOS) and partial density of state (PDOS) site projected for both compounds are calculated using both methods PBE-GGA and TB-mBJ. The TDOS and PDOS for $BaZrO_3$ are shown in figure 4. It is clear that the lower valence band consist of Ba-*p* state around -10.1 to -11 eV, and the upper valence band extends down to approximately -4 eV and is composed mainly of O-*p* states with a small contribution from Zr-*d* states, while the lower conduction band is mainly a mixture of Ba-*d* and Zr-*d* states, with a small admixture from O-*p*. In the conduction bands, the Zr-d states are dominant. Figure 5 displays the TDOS and PDOS for $BaHfO_3$ perovskite using both PBE-GGA and TB-mBJ methods. The contribution to the lowest valence band at −10 eV is due to Ba-*p* state, whereas the upper valence band (around -4.2 to 0 eV) is from O-*p* states hybridized with some Hf-*p* and Hf-*d* electrons. The bands above the Fermi level are the conduction band of the compound; the lower part of the band (around 3.8 to 6 eV) is dominated by the O-*p*. Also, it can be seen from the plot, the top of consist are mainly Ba-*d* and Hf-*d* states hybridized with some O-*p*. The conduction bands are composed mostly of antibonding between Hf-*d* and O-*p* as well as antibonding between Ba-*d* and O-*p*, maximum peak at 7.5 eV is due to the unoccupied *d* states of Hf.

3.3 Optical Properties

In this subsection, the optical characteristics of $BaHfO_3$ and $BaZrO_3$ are presented. Electronic excitations will take place within the crystal if it is exposed to electromagnetic radiation. As a result, the optical features of the crystal will be observed. The nature of the response to an incident electromagnetic wave at a particular frequency determines if this material could be used in optoelectronic devices. The different optical characteristics of the crystals are mainly calculated by using the frequency-dependent complex dielectric tensor $\varepsilon^{ij}(\omega)$. Since $BaZrO_3$ and $BaHfO_3$ perovskites has cubic structure symmetry which means one tensor component is enough to do optical calculations. Thus, the optical characteristics of the materials $n(\omega)$, $k(\omega)$, $R(\omega)$, $\sigma(\omega)$, $\alpha(\omega)$, and $L(\omega)$ could be derived from their $\varepsilon_1(\omega)$ and $\varepsilon_2(\omega)$ values as illustrated in the computational details section [48].

The imaginary part $\varepsilon_2(\omega)$ is determined from the electronic structure through the joint density of states and the momentum matrix elements between the occupied and the unoccupied wave functions within the selection rules. In figure 6, the optical characteristics for both $BaZrO_3$ and $BaHfO_3$ compounds are plotted. In panel a) the spectrum of $\varepsilon_2(\omega)$ shows the three peaks structure for $BaZrO_3$ and $BaHfO_3$. The $\varepsilon_2(\omega)$ has deeply impact on the absorption spectrum of the matter. A large value of $\varepsilon_2(\omega)$ refers to a large absorption spectrum include of the whole of all different transitions that will occur between the valance and the conduction bands. It is starting to response to the incident radiation at critical points which are the threshold energy at 2.87 eV and 4.26 eV for $BaZrO_3$ and $BaHfO_3$ respectively. These points are Cv–Cc splitting and give a threshold for indirect optical transitions between the highest valance band and the lowest conduction band. This is known as the fundamental absorption edge. The main peak in the spectrum is situated at 7.12 eV and 7.52 eV for $BaZrO_3$, and $BaHfO_3$, respectively. These peaks are dominated by transitions from the O-*p* band and the small contribution of transition metals *d* state just below Fermi energy to Ba-*p* state of the conduction band. In panel b) the spectrum of $\varepsilon_1(\omega)$ for $BaZrO_3$ and $BaHfO_3$ compounds show that the static dielectric constant $\varepsilon_1(0)$ are equal 3.69 and 3.51, whereas the main peaks appear at energy 5.24 eV and 5.59 eV, respectively. It is important to consider both ε_1 and ε_2 together since they affect each other, meaning the shape of ε_2 cause corresponding changes in the shape of ε_1 and vice-versa. This is known as the Kramers-Kronig relation between the real (ε_1) and imaginary (ε_2) parts of the dielectric function. In short, the dielectric function describes what an electric field such as an oscillating light wave does to the material. In panel c) the absorption coefficients for $BaZrO_3$ and $BaHfO_3$ compounds show the same behavior as $\varepsilon_2(\omega)$. The absorption edges start from 3.28 and 4.29 eV for $BaZrO_3$ and $BaHfO_3$ respectively which are corresponding to optical bandgaps. This produces from the transition of the O-p valence band electrons to the empty d conduction bands in Zr or Hf. In $BaHrO_3$ perovskite, the main peak in dielectric absorption spectra occurs at 7.81 eV whereas the two other peaks at 11.3 and 11.78 eV whereas in $BaZrO_3$ the main peak occurs at 7.31 eV the other two peaks occur at 8.8 and 11.0 eV. In both compounds, the Ba does not contribute to the low-energy absorption spectra; because its electron valence bands are not in the transition energy

domain. In panel d) the loss function for $BaZrO_3$ and $BaHfO_3$ compounds are plotted and their peaks occur at 7.6 eV and 8.4 eV, respectively. In panel e) the reflectivity for both $BaZrO_3$ and $BaHfO_3$ compounds are plotted and their static reflectivity $R(0)$ is approximately equal 10%. At low energies (i.e., 0–7.8 eV for $BaHfO_3$ and 0–7.2 eV for $BaZrO_3$), the reflectivity spectrum was observed to extend as high as 33% and 30% for $BaHfO_3$ and $BaZrO_3$, respectively. Our calculations show a strong reflectivity at high energies increase up to 75%, and 72% for $BaHfO_3$, and $BaZrO_3$, respectively. In panel f) the refractive index plots show that the static refractive index $n(0)$ are equal 1.92 and 1.87 for $BaZrO_3$ and $BaHfO_3$, respectively. The refractive index reaches its maximum value 2.7 at 7.5 eV for $BaHfO_3$, whereas for $BaZrO_3$ its 2.5 occurs at 5.0 eV.

Finally, the optical conductivity $\sigma(\omega)$ for both $BaZrO_3$ and $BaHfO_3$ perovskites are displayed in figure 7. There is quite similarity in curves of both perovskites. For $BaZrO_3$ the first peak appears at 6.8 eV, the second peak appears at 9.0 eV whereas the third peak at 10.5 eV. On the other hand, at $BaHfO_3$ there are two mean peaks at 7.4 eV and 11.5 eV. The maximum value for $BaZrO_3$ is equal 8900 at 10.5 eV while for $BaHfO_3$ it is equal 9100 at 11.5 eV.

3.4 Thermoelectric (TE) Properties

The efficient thermoelectric characteristics for any materials determines by their figure of merit $zT = S^2\sigma T/\kappa^{\circ}$, the increasing of S and σ increase figure of merit while increasing κ° decrease figure of merit. As we known, a suitable material for thermoelectric applications should have figure of merit equal or greater than one which give energy transformation efficiency greater than 25% [49].

Figure 8 shows the variation of Seebeck coefficient S with respect to temperature for both compounds $BaZrO_3$ and $BaHfO_3$. The two curves have the approximately same behavior where they change nonlinearly by increasing from zero to reach the maximum value 206.86 μV/K at T=270K for $BaZrO_3$ and 288.13 μV/K at T=180K for $BaHfO_3$, after that it is decreasing slightly in $BaHfO_3$ but in $BaZrO_3$ it is still increasing. At room temperature (RT), Seebeck coefficients for $BaZrO_3$ and $BaHfO_3$ are 208 and 261 μV/K, respectively. In figure 9, the electric conductivity σ as a function of temperature when the constant relaxation time $\tau_0 = 0.8 \times 10^{-14}s$ is used, it is shown that the electric conductivity is decreasing non-linearly at the low temperature to reach its global minimum at T=121K in $BaZrO_3$ case and T=90 in $BaHfO_3$, then it starts increasing linearly with temperature increases for both $BaZrO_3$ and $BaHfO_3$. The electric conductivity at RT for $BaZrO_3$ is about $0.554 \times 10^5 S/m$ and it about $0.289 \times 10^5 S/m$ for $BaHfO_3$. Figure 10 displays the electronic thermal conductivity κ^0 as a function of temperature when the constant relaxation time $\tau_0 = 0.8 \times 10^{-14}s$ is used. The behavior of the electronic thermal conductivity curves are nonlinear increasing for both compounds. The electronic thermal conductivity of $BaHfO_3$ at RT is equal to 0.154 $Wm^{-1}K^{-1}$, which is about half the $BaZrO_3$ value of 0.309 $Wm^{-1}K^{-1}$. Our results contradict the previous experimental values 10.4 [50] and 5.2 [51] Wm^{-}

$^{1}K^{-1}$, respectively. This contradicts maybe because we calculated only the electronic part of thermal conductivity but the experiment results were for total thermal conductivity where the lattice part was dominant in both compounds. The temperature dependence of the thermal conductivities of $BaZrO_3$ and $BaHfO_3$ follow an inverse temperature law (1/T) at low temperatures, showing typical phonon conduction characteristics [51].

Figure 11 shows how are the power factor (PF) curves changed when the temperature increase for both compounds. They reach their maximum values 0.213 $\mu W/mk^2$ at T=180K for $BaHfO_3$ and 0.0814 $\mu W/mk^2$ at T=240K for $BaZrO_3$. Also, at RT the PF's equal 0.128 $\mu W/mk^2$ for $BaHfO_3$ and 0.0778 $\mu W/mk^2$ for $BaZrO_3$. Although the PF values for both compounds are very small if they compared with the well-known thermoelectric materials but the results show that $BaHfO_3$ is better than $BaHfO_3$ if a suitable dopant used.

To determine in details thermoelectric (TE) behavior for both $BaHfO_3$and $BaZrO_3$, such as Seebeck coefficient (S), electrical conductivity (σ), power factor (PF), electronic specific heat (C_e), and electronic thermal conductivity (κ°) have been expressed as a function of chemical energy (μ); the calculated characteristics were plotted for considered temperatures: 300 – 800 K. In figure 12, the Seebeck coefficients S for both $BaZrO_3$ and $BaHfO_3$ compounds as a function of chemical energy μ at different temperature are plotted. For both compounds, the curve increases linearly from zero value to reach the maximum value and then decreases sharply to negative global minimum values after that it increases linearly again to reach zero value.

The chemical potential dependencies of electric conductivity rate (σ/τ) for both $BaZrO_3$ and $BaHfO_3$ compounds at different temperatures are depicted in figure 13 panels a) and b). In the two panels, the electric conductivity goes to zero in energy range 0.52 – 0.74 Ry for $BaZrO_3$ and 0.54 – 0.8 Ry for $BaHfO_3$ for the wide range of temperatures from 200K to 800K. In figure 14 the power factor with respect to chemical energy at different temperature are plotted for $BaZrO_3$ and $BaHfO_3$ perovskites. The two plots display two main peaks 11.7 $\times 10^{11}$ W/mK^2s and 6.0 $\times 10^{11}$ W/mK^2s at 0.525 Ry and 0.83 Ry for $BaZrO_3$ respectively, and 10.65 $\times 10^{11}$ W/mK^2s and 6.75 $\times 10^{11}$ W/mK^2s at 0.5 Ry and 0.775 Ry for $BaHfO_3$ respectively. Figure 15 shows the electronic specific heat capacity as a function of chemical energy at different temperature. Cordfunke and Konings have estimated the heat capacity at room temperature from a comparison with $BaZrO_3$and recommended 101.7 J $K^{-1}mol^{-1}$at 298.15 K [52]. The calculated heat capacity of $BaZrO_3$ in this study is well agreement with the data in the literature [52,53]. Figure 16 shows the variation of the density of state around the Fermi level with respect of temperature. For the two alloys $BaZrO_3$ and $BaHfO_3$ the band gap still appear for a wide range of temperature.

4. Conclusions

Employing the all-electrons full-potential LAPW method based on DFT, with using PBE-GGA functional of exchange-correlation energy; and semi-local exchange potential TB-mBJ to study

physical properties. Also, semi-classical Boltzmann transport theory has been used. The structural, electronic, optical properties, as well as the transport properties of $BaZrO_3$ and $BaHfO_3$, have been studied. A summary of results are:

(i) The calculated lattice constants at zero pressure of these compounds are in a reasonable agreement with the previous theortical and experimental values.

(ii) The electronic bandstructure calculations showed that $BaZrO_3$ and $BaHfO_3$ are insulators materials with an indirect bandgap ($R-\Gamma$). The fundamental bandgap of this compounds increases when mBJ-GGA approach is used instead of PBE-GGA.

(iii) The joint DOS and the Kramers-kronig transformation are used to calculate and analyze the optical characteristics: dielectric constant$\varepsilon(\omega)$, the absorption coefficient$\alpha(\omega)$, the reflectivity$R(\omega)$, the refractive index $n(\omega)$ and electron loss energy$L(\omega)$. The oxygen *p* states and Transition metals Zr- and Hf-*d* states play a major role in optical transitions.

(iv) Finally, The calculated transport characteristics showed that the two compounds are not suitable choice for thermoelectric applications but if they dopant with some impurities their properties could be improved.

References

1. Tian, H. Y. *et al.* Synthesis of $BaZr_{0.75}Hf_{0.25}O_3$ by a solid-state reaction technique and characterizations of dielectric properties. *J. Alloys Compd.* **402**, 251–255 (2005).

2. Bandura, A. V, Evarestov, R. A. & Kuruch, D. D. Hybrid HF-DFT modeling of monolayer water adsorption on (001) surface of cubic $BaHfO_3$ and $BaZrO_3$ crystals. *Surf. Sci.* **604**, 1591–1597 (2010).

3. H. Stetson & B. Schwartz. Dielectric Properties of Zirconates. *Joutnal Am. Ceram. Soc.* **44**, 420 (1961).

4. Zhang, J. L. & Evetts, J. E. $BaZrO_3$ and $BaHfO_3$: preparation, properties and compatibility with $YBa_2Cu_3O_{7-x}$. *J. Mater. Sci.* **29**, 778 (1994).

5. Megaw, H. D. Crystal structure of double oxides of the perovskite type. *Proc. Phys. Soc.* **58**, 133–152 (1946).

6. Scholder, R., Rade, D. & Schwarz, H. Uber Zirkonate, Hafnate und Thorate von Barium, Strontium, Lithium und Natrium. *Zeitschrift Anorg. und Allg. Chemie* **362**, 149–168 (1968).

7. P. Turlier U. M. Pretthe, C. R. hebd. No Title. *Séances Acad. Sci.* **248**, 2572 (1959).

8. King-Smith', R. D. & Vanderbilt, D. First-principles investigation of ferroelectricity in perovskite compounds. *Phys. Rev. B* **49**, 5828 (1994).

9. Dash, S., Sood, D. D. & Prasad, R. Phase diagram and thermodynamic calculations of alkali and alkaline earth metal zirconates. *J. Nucl. Mater.* **228**, 83–116 (1996).

10. Iles, N. *et al.* Atomistic study of structural, elastic, electronic and thermal properties of perovskites Ba(Ti,Zr,Nb)O_3. *Comput. Mater. Sci.* **39**, 896–902 (2007).

11. Bouhemadou, A., Djabi, F. & Khenata, R. First principles study of structural, elastic, electronic and optical properties of the cubic perovskite $BaHfO_3$. *Phys. Lett. Sect. A Gen. At. Solid State Phys.* **372**, 4527–4531 (2008).

12. Evarestov, R. A. Hybrid density functional theory LCAO calculations on phonons in Ba(Ti,Zr,Hf)O_3. *Phys. Rev. B - Condens. Matter Mater. Phys.* **83**, 014105 (2011).

13. Verma, A. S. & Kumar, A. Bulk modulus of cubic perovskites. *J. Alloys Compd.* **541**, 210–214 (2012).

14. Zhao, H., Chang, A. & Wang, Y. Structural, elastic, and electronic properties of cubic perovskite $BaHfO_3$ obtained from first principles. *Phys. B Condens. Matter* **404**, 2192–2196 (2009).

15. Ali, Z., Khan, I., Ahmad, I., Khan, M. S. & Asadabadi, S. J. Theoretical studies of the paramagnetic perovskites $MTaO_3$ (M = Ca, Sr and Ba). *Mater. Chem. Phys.* **162**, 308–315 (2015).

16. Mubarak, A. A. & Mousa, A. A. The electronic and optical properties of the fluoroperovskite $BaXF_3$ (X = Li, Na, K, and Rb) compounds. *Comput. Mater. Sci.* **59**, 6–13 (2012).

17. Nakashima, K. *et al.* Preparation of BaZrO3 nanoparticles using a solvothermal reaction. in *IOP Conference Series: Materials Science and Engineering* vol. 18 (Institute of Physics Publishing, 2011).

18. Khenata, R. *et al.* First-principle calculations of structural, electronic and optical properties of $BaTiO_3$ and $BaZrO_3$ under hydrostatic pressure. *Solid State Commun.* **136**, 120–125 (2005).

19. Vali, R. Lattice dynamics and electronic properties of the scintillator host material: Barium hafnate. *Solid State Commun.* **147**, 1–3 (2008).

20. Abrutis, A. *et al.* Chemical vapor deposition and characterization of high-k $BaHf_{1-x}Ti_xO_3$ dielectric layers for microelectronic applications. *J. Vac. Sci. Technol. B, Nanotechnol. Microelectron. Mater. Process. Meas. Phenom.* **29**, 01A303 (2011).

21. Borja-Urby, R. *et al.* Structural study, photoluminescence, and photocatalytic activity of semiconducting $BaZrO_3$:Bi nanocrystals. in *Materials Science and Engineering B: Solid-State Materials for Advanced Technology* vol. 176 1382–1387 (2011).

22. Parida, S. *et al.* Structural refinement, optical and microwave dielectric properties of $BaZrO_3$. *Ceram. Int.* **38**, 2129–2138 (2012).

23. Khan, Z. & Qureshi, M. Tantalum doped $BaZrO_3$ for efficient photocatalytic hydrogen generation by water splitting. *Catal. Commun.* **28**, 82–85 (2012).

24. Zhang, Y., Liu, M., Wang, J., Shimada, T. & Kitamura, T. Strain tunable ferroelectric and dielectric properties of $BaZrO_3$. *J. Appl. Phys.* **115**, 224107 (2014).

25. Chen, T. *et al.* One-step synthesis of hollow $BaZrO_3$ nanocrystals with oxygen vacancies for photocatalytic hydrogen evolution from pure water. *J. Alloys Compd.* **780**, 498–503 (2019).

26. Meng, J. *et al.* $BaZrO_3$ hollow nanostructure with Fe (III) doping for photocatalytic hydrogen evolution under visible light. *Int. J. Hydrogen Energy* **43**, 9224–9232 (2018).

27. Khirade, P. P., Birajdar, S. D., Shinde, A. B. & Jadhav, K. M. Room temperature ferromagnetism and photoluminescence of multifunctional Fe doped $BaZrO_3$ nanoceramics. *J. Alloys Compd.* **691**, 287–298 (2017).

28. Perdew, J. P., Burke, K. & Ernzerhof, M. Generalized Gradient Approximation Made Simple. *Phys. Rev. Lett.* **77**, 3865 (1996).

29. Becke, A. D. & Johnson, E. R. A simple effective potential for exchange. *J. Chem. Phys.* **124**, 221101 (2006).

30. Tran, F. & Blaha, P. Accurate band gaps of semiconductors and insulators with a semilocal exchange-correlation potential. *Phys. Rev. Lett.* **102**, 226401 (2009).

31. Hohenberg, P. & Kohn, W. Inhomogeneous Electron Gas. *Phys. Rev.* **136**, B864 (1964).

32. Kohn, W. Density Functional and Density Matrix Method Scaling Linearly with the Number of Atoms. *Phys. Rev. Lett.* **76**, 3168 (1996).

33. Cottenier, S. *Density Functional Theory and the family of (L)APW-methods: a step-by-step introduction*. 2nd ISBN 978-90-807215-1-7 (freely available at http://www.wien2k.at/reguser/textbooks) (2013).

34. Krogh Andersen, O. Linear methods in band theory*. *Phys. Rev. B* **12**, 3060 (1975).

35. Singh, D. J. & Nordström, L. *Planewaves, pseudopotentials and the LAPW method*. (Springer Science & Business Media, 2006).

36. Blaha, P. *et al.* WIEN2k: An APW+lo program for calculating the properties of solids. *J. Chem. Phys.* **152**, 074101 (2020).

37. Frederick Wooten. *Optical Properties of Solids*. (Academic Press, 1972).

38. Smith, N. V. Photoelectron Energy Spectra and the Band Structures of the Noble Metals. *Phys. Rev. B* **3**, 1862–1878 (1971).

39. Mark Fox. *Optical Properties of Solids*. (Oxford University Press, 2010).

40. M. Dreesel & G. Gruner. *Electrodynamics of Solids: Optical Properties of Electrons in*

Matter. (Cambridge University Press, 2002).

41. Madsen, G. K. H. & Singh, D. J. BoltzTraP. A code for calculating band-structure dependent quantities. *Comput. Phys. Commun.* **175**, 67–71 (2006).

42. Khandy, S. A. & Gupta, D. C. Investigation of structural, magneto-electronic, and thermoelectric response of ductile $SnAlO_3$ from high-throughput DFT calculations. *Int. J. Quantum Chem.* **117**, e25351 (2017).

43. Cutler, M. & Mott, N. F. Observation of Anderson localization in an electron gas. *Phys. Rev.* **181**, 1336–1340 (1969).

44. P Drude. Zur Elektronentheorie der Metalle. *Ann. Phys.* **306**, 566 (1900).

45. Ashcroft, N. W. & Mermin, N. D. *Solid state physics*. (Philadelphia, saunders college, 1976).

46. Bhalla, A. S., Guo, R. & Roy, R. The perovskite structure—a review of its role in ceramic science and technology. *Mater. Res. Innov.* **4**, 3–26 (2000).

47. Birch, F. Elasticity And Constitution Of The Earth's Interior. *J. Geophys. Res.* **57**, 227-286 (1952).

48. Chanda, S. *et al.* Calculations of the structural and optoelectronic properties of cubic $Cd_xZn_{1-x}Se_yTe_{1-y}$ semiconductor quaternary alloys using the DFT-based FP-LAPW approach. *J. Comput. Electron.* **19**, 1-25 (2020).

49. Alrahamneh, M. J., Mousa, A. A. & Khalifeh, J. M. First principles study of the structural, electronic, magnetic and thermoelectric properties of Zr_2RhAl. *Phys. B Condens. Matter* **552**, 227–235 (2019).

50. Maekawa, T., Kurosaki, K. & Yamanaka, S. Thermal and mechanical properties of perovskite-type barium hafnate. *J. Alloys Compd.* **407**, 44–48 (2006).

51. Yamanaka, S. *et al.* Thermophysical properties of $BaZrO_3$ and $BaCeO_3$. *J. Alloys Compd.* **359**, 109–113 (2003).

52. Cordfunke, E. H. P. & Konings, R. J. M. *Thermochemical Data for Reactor Materials and Fission Products*. The ECN database. *Journal of Phase Equilibria 14, 457-464* (1993).

53. Kurosaki, K., Konings, R. J. M., Wastin, F. & Yamanaka, S. The low-temperature heat capacity and entropy of $SrZrO_3$ and $BaZrO_3$. *J. Alloys Compd.* **424**, 1–3 (2006).

54. Stenstrop, G. & Engell, J. $BaZrO_3$: Synthesis, Properties and Compatibility with $Ba_2YCu_3O_{7-x}$. *J. Less-Common Metah*, **164**, 200–207 (1990).

55. Azad, A.-M. & Subramaniam, S. Synthesis of $BaZrO_3$ by a solid-state reaction technique using nitrate precursors. *Mater. Res. Bull.* **37**, 85 (2002).

56. Yamanaka, S. *et al.* Heat capacities and thermal conductivities of perovskite type $BaZrO_3$ and $BaCeO_3$. *J. Alloys Compd.* **359**, 1–4 (2003).

57. Moreira, M. L., Andrés, J., Varela, J. A. & Longo, E. Synthesis of fine micro-sized $BaZrO_3$ powders based on a decaoctahedron shape by the microwave-assisted hydrothermal method. *Cryst. Growth Des.* **9**, 833–839 (2009).

58. Gallucci, K., Villa, P., Groppi, G., Usberti, N. & Marra, G. Catalytic combustion of methane on $BaZr_{(1-x)}Me_xO_3$ perovskites synthesised by a modified citrate method. *Catal. Today* **197**, 236–242 (2012).

59. Terki, R., Feraoun, H., Bertrand, G. & Aourag, H. Full potential calculation of structural, elastic and electronic properties of $BaZrO_3$ and $SrZrO_3$. *Phys. status solidi* **242**, 1054–1062 (2005).

60. Sundell, P. G., Björketun, M. E. & Wahnström, G. Thermodynamics of doping and vacancy formation in $BaZrO_3$ perovskite oxide from density functional calculations. *Phys. Rev. B - Condens. Matter Mater. Phys.* **73**, 104112 (2006).

61. Sahoo, M. P. K., Zhang, Y. & Wang, J. Enhancement of ferroelectric polarization in layered $BaZrO_3/BaTiO_3$ superlattices. *Phys. Lett. A* **380**, 299–303 (2016).

62. López Garciá, A. R., de la Presa, P. & Rodríguez, A. M. Temperature dependence of the hyperfine interaction in the cubic phase of $BaHfO_3$. *Phys. Rev. B* **44**, 9708–9710 (1991).

63. Alonso, R. E., Horowitz, C., López García, A., Lamas, D. G. & Caneiro, A. Second order tetragonal-to-cubic phase transition in $Sr_{0.5}Ba_{0.5}HfO_3$. *Solid State Commun.* **120**, 205–210 (2001).

64. Li, L., Kennedy, B. J., Kubota, Y., Kato, K. & Garrett, R. F. Structures and phase transitions in $Sr_{1-x}Ba_xHfO_3$ perovskites. *J. Mater. Chem.* **14**, 263–273 (2004).

65. Feteira, A., Sinclair, D. C., Rajab, K. Z. & Lanagan, M. T. Crystal structure and microwave dielectric properties of alkaline-earth hafnates, $AHfO_3$(A=Ba, Sr, Ca). in *Journal of the American Ceramic Society* vol. 91 893–901 (Blackwell Publishing Inc., 2008).

66. Yu, X., Chen, G.-F., Shen, J., Li, Y.-X. & Luo, X.-G. First principle calculation of structural, elastic and electronic properties of $XHfO_3$(X=Ba, Sr). *Acta Phys. Sin.* **56**, 5366–5370 (2007).

67. Liu, Q. J., Liu, Z. T., Feng, L. P. & Tian, H. Mechanical, electronic, chemical bonding and optical properties of cubic $BaHfO_3$: First-principles calculations. *Phys. B Condens. Matter* **405**, 4032–4039 (2010).

68. Azahaf, C., Zaari, H., Abbassi, A., Ez-Zahraouy, H. & Benyoussef, A. Theoretical investigation of spontaneous polarization, electronic and optical properties of cubic perovskite $BaHfO_3$. *Opt. Quantum Electron.* **47**, 2889–2897 (2015).

69. Yangthaisong, A. Electronic and lattice vibrational properties of cubic $BaHfO_3$ from first principles calculations. *Phys. Lett. Sect. A Gen. At. Solid State Phys.* **377**, 927–931 (2013).

70. Robertson, J. Band offsets of wide-band-gap oxides and implications for future electronic

devices. *J. Vac. Sci. Technol. B Microelectron. Nanom. Struct.* **18**, 1785–1791 (2000).

Table caption

Table1: Lattice constant α(Å), bulk modulus B(GPa), for the perovskties $BaZrO_3$ and $BaHfO_3$.

Compound	α(Å)	B(GPa)	Method
$BaZrO_3$	4.234	149.8	This work
	4.189[5], 4.193[54], 4.19[6,8,55], 4.192[4,51,56], 4.2269[10], 4.2063[57], 4.1812[22], 4.1815[58], 4.193[27]	103[51,56], 155.9[10], 127[13]	Exp
	4.154[8],4.207[59], 4.148[18], 4.25[60], 4.193[13], 4.16[24,61], 4.19[2], 4.198[12]	175.3[8],157, 174.7[18], 141[13], 172[2], 168[12]	Theory
$BaHfO_3$	4.212	156.0	This work
	4.171[4,6,50], 4.17[62], 4.172[63], 4.1668[64], 4.1796[65],		Exp
	4.171[13], 4.19[2], 4.193[12], 4.310[66], 4.2499[11], 4.170[19], 4.286[14], 4.248[67], 4.160[68], 4.064[69]	144[13], 175[2], 171[12], 123.6[66], 186[11a], 194[11b], 146.72[14a], 145.50[14b], 179[69]	Theory

[11a, 14a] Obtained from the Voigt–Reuss–Hill (VRH) approximation.

[11b, 14b] Obtained from fitting the third-order Birch–Murnaghan equation

Table 2: The calculated bandgap (Eg) using PBE-GGA and TB-mBJ methods with comparison with previous computational and experimental results

$BaZrO_3$			**$BaHfO_3$**		
E_g (eV)	method	Ref.	E_g (eV)	method	Ref.
4.42	TB-mBJ	This work	5.25	TB-mBJ	This work
3.39	PBE-GGA	This work	3.69	PBE-GGA	This work
5.3	Exp.	[70]	6	Exp	[19]
3.9	LDA	[18]	2.99	LDA	[11]
3.156	GGA	[10]	3.94	SX-LDA	[14]
5.4	LCAO	[12]	3.17	GGA	[14]
3.55	Exp.	[22]	5.3	SX-LDA	[69]
4.96	Exp.	[26]	3.9	GGA-PBE	[68]
			5.9	TB-mBJ	[68]

Figure Captions:

Figure1: Crystal structures of $BaTMO_3$ (TM: blue, Ba: green and O: red).
Figure2: Band structure of cubic perovskite $BaZrO_3$ using a) PBE-GGA and b) TB-mBJ methods.
Figure3: Band structure of cubic perovskite $BaHfO_3$ using a) PBE-GGA and b) TB-mBJ methods.
Figure4: Calculated total and Partial-projected DOS for $BaZrO_3$ using PBE-GGA compared with TB-mBJ method.
Figure5: Calculated total and Partial-projected DOS for $BaHfO_3$ using PBE-GGA compared with TB-mBJ method.
Figure6: Calculated optical properties for the $BaHfO_3$ and $BaZrO_3$ compounds, a) $\varepsilon_2(\omega)$, b) $\varepsilon_1(\omega)$, c) $\alpha(\omega)$, d) $L(\omega)$, e) $R(\omega)$, and f) $n(\omega)$.
Figure7: Calculated optical conductivity $\sigma(\omega)$ for $BaHfO_3$ and $BaZrO_3$
Figure8: Seebeck coefficient as a function of temperature at ground state chemical potential for the $BaHfO_3$ and $BaZrO_3$ compounds.
Figure9: The electrical conductivity rate (σ/τ) as a function of temperature at ground state chemical potential for the $BaHfO_3$ and $BaZrO_3$ compounds.
Figure10: The electronic thermal conductivity κ^0 as a function of temperature at ground state chemical potential.
Figure11: The power factor (PF) as a function of temperature.
Figure 12: Seebeck coefficient S as a function of chemical potential at different temperature for a) $BaHfO_3$ and b) $BaZrO_3$.
Figure13: (a) and (b) are the electrical conductivity rate (σ/τ) as a function of chemical potential at different temperature for both $BaHfO_3$ and $BaZrO_3$; (c) and (d) are the electronic thermal conductivity as a function of chemical potential at different temperature for both compounds $BaHfO_3$ and $BaZrO_3$, respectively.
Figure14: The power factor ($PF = S^2\sigma/\tau$) as a function of chemical potential at different temperature for a) $BaHfO_3$ and b) $BaZrO_3$.
Figure15: The electronic specific heat as a function of chemical potential at different temperature for a) $BaHfO_3$ and b) $BaZrO_3$.
Figure 16: The density of state at Fermi level $DOS[E_F]$ as a function of chemical potential at different temperature for a) $BaHfO_3$ and b) $BaZrO_3$.

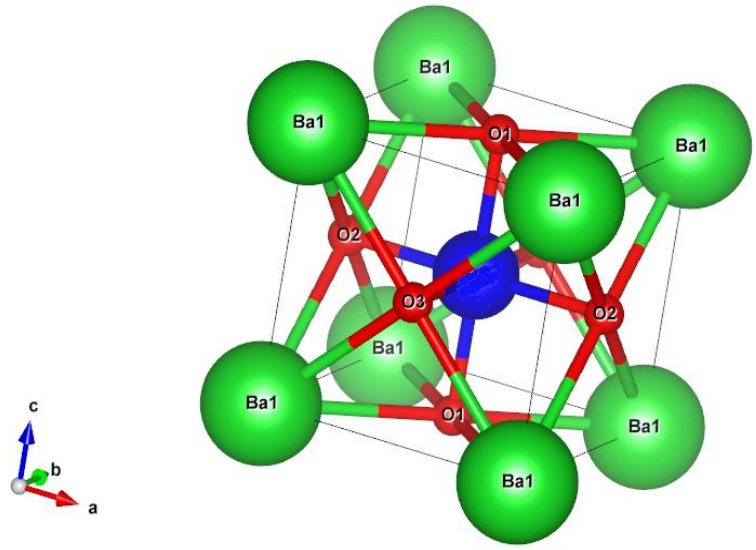

Figure1

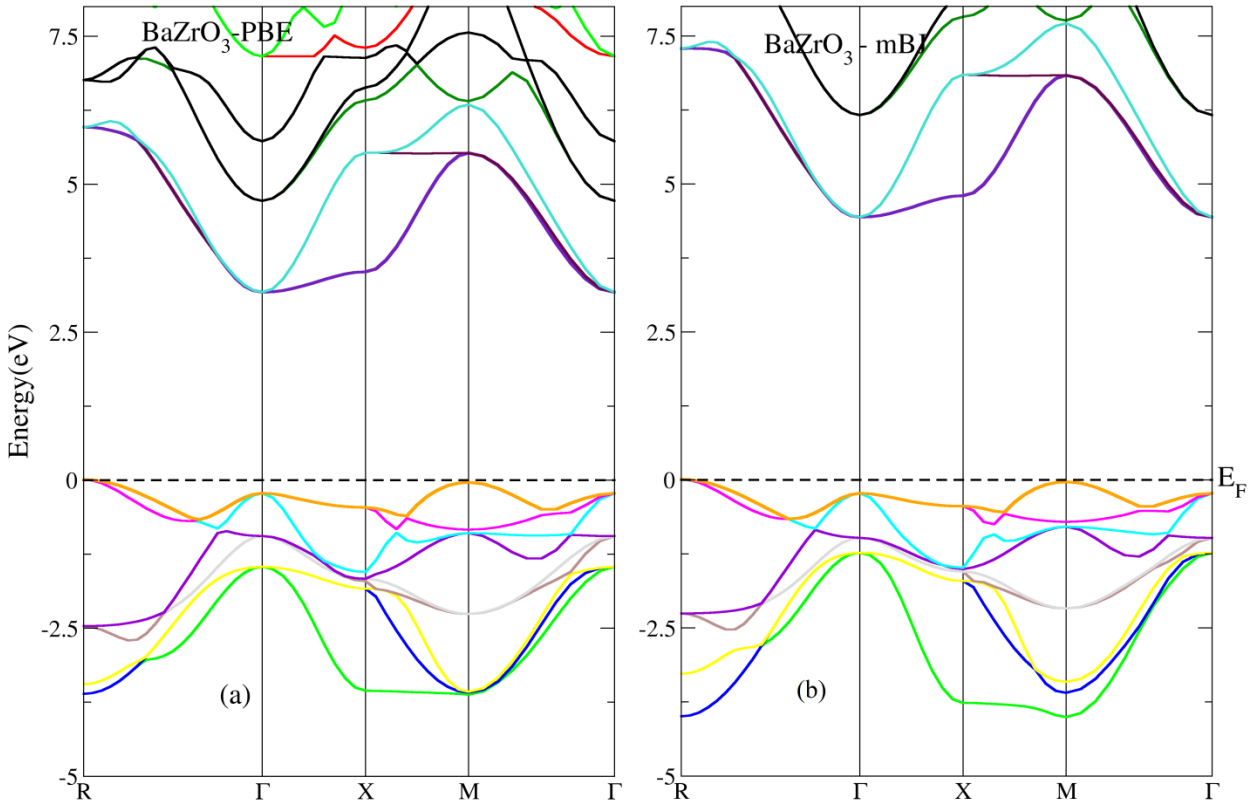

Figure 2

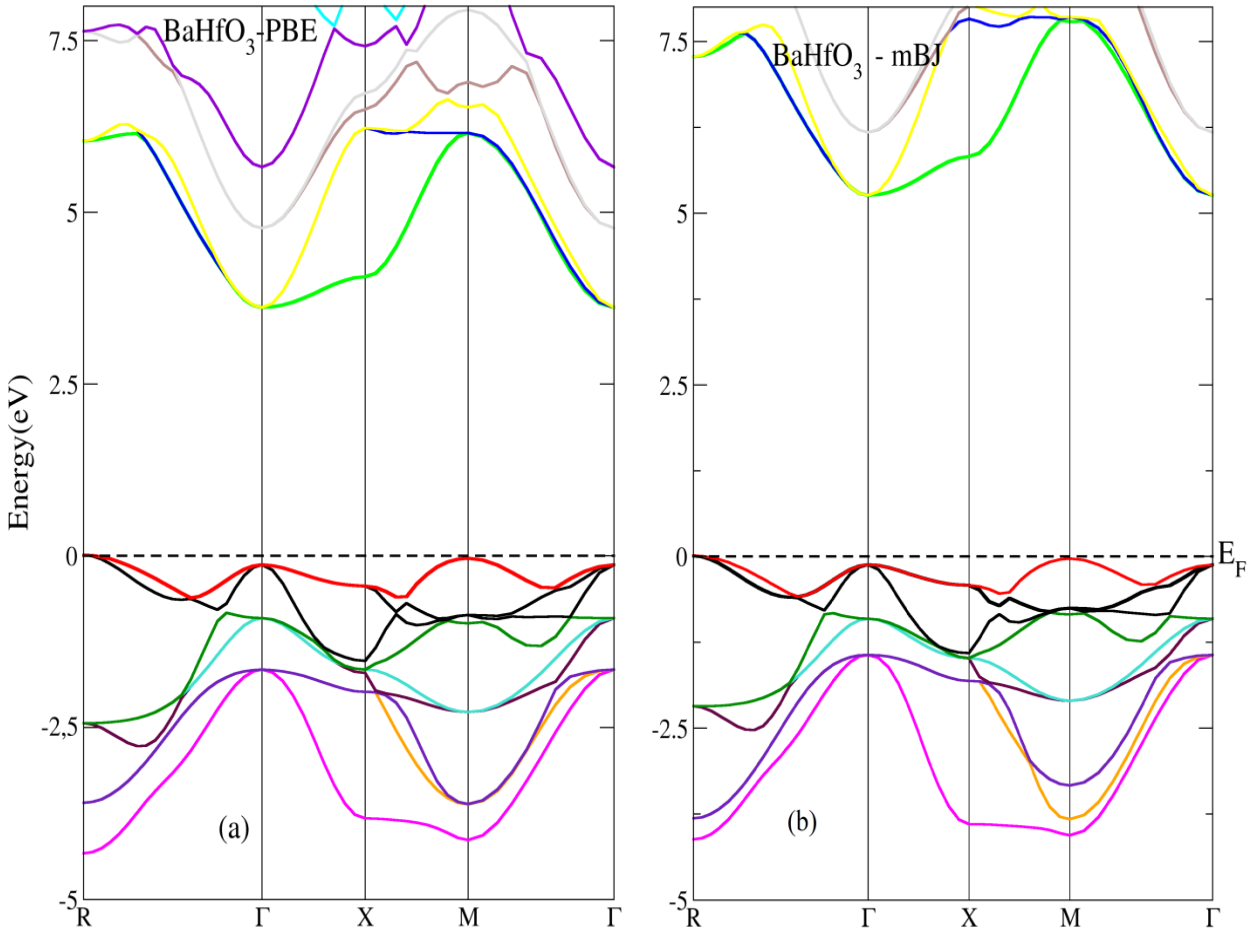

Figure3

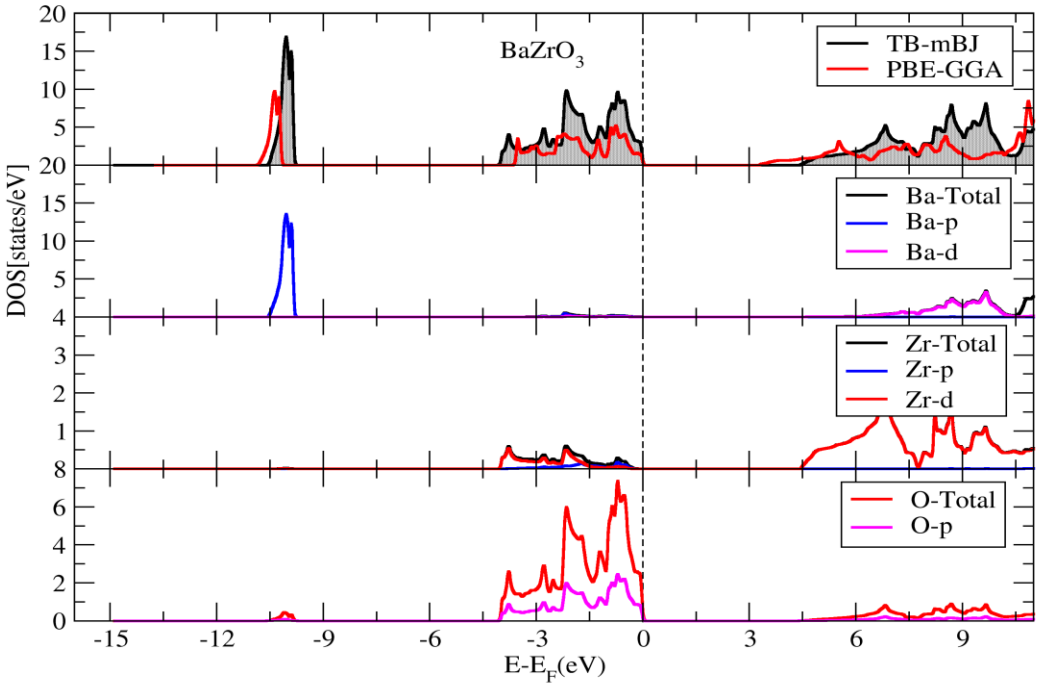
BaZrO3
TB-mBJ
PBE-GGA
Ba-Total
Ba-p
Ba-d
Zr-Total
Zr-p
Zr-d
O-Total
O-p
DOS[states/eV]
E-EF(eV)

Figure 4

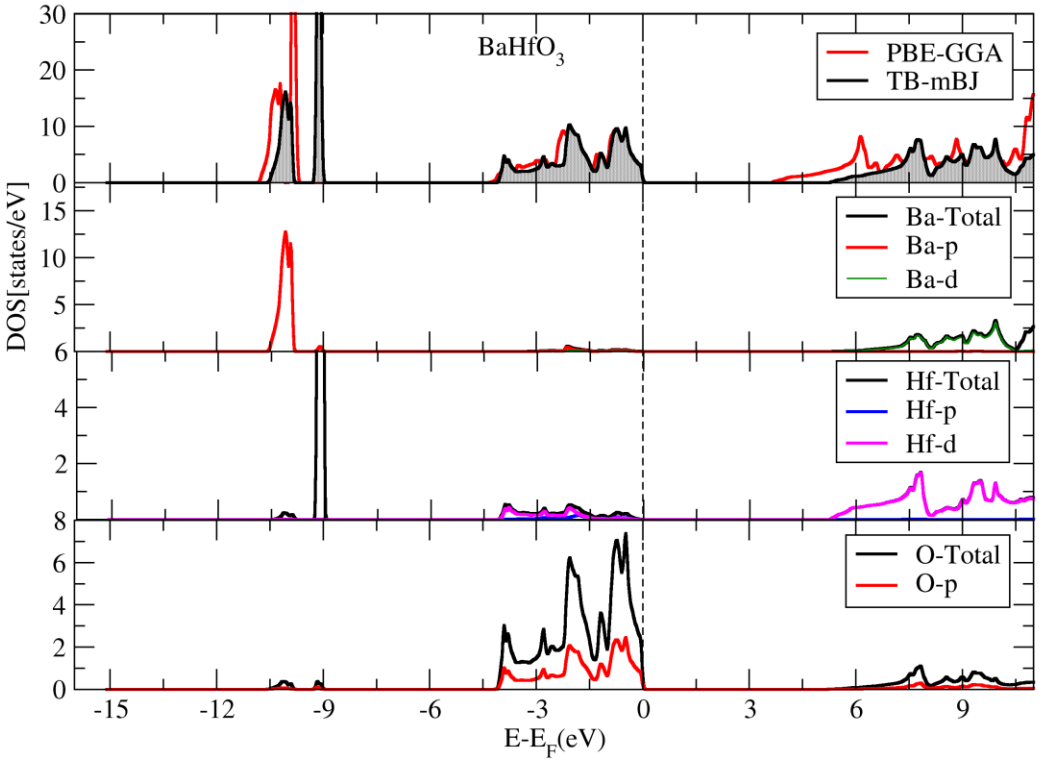
BaHfO3
PBE-GGA
TB-mBJ
Ba-Total
Ba-p
Ba-d
Hf-Total
Hf-p
Hf-d
O-Total
O-p
DOS[states/eV]
E-EF(eV)

Figure 5

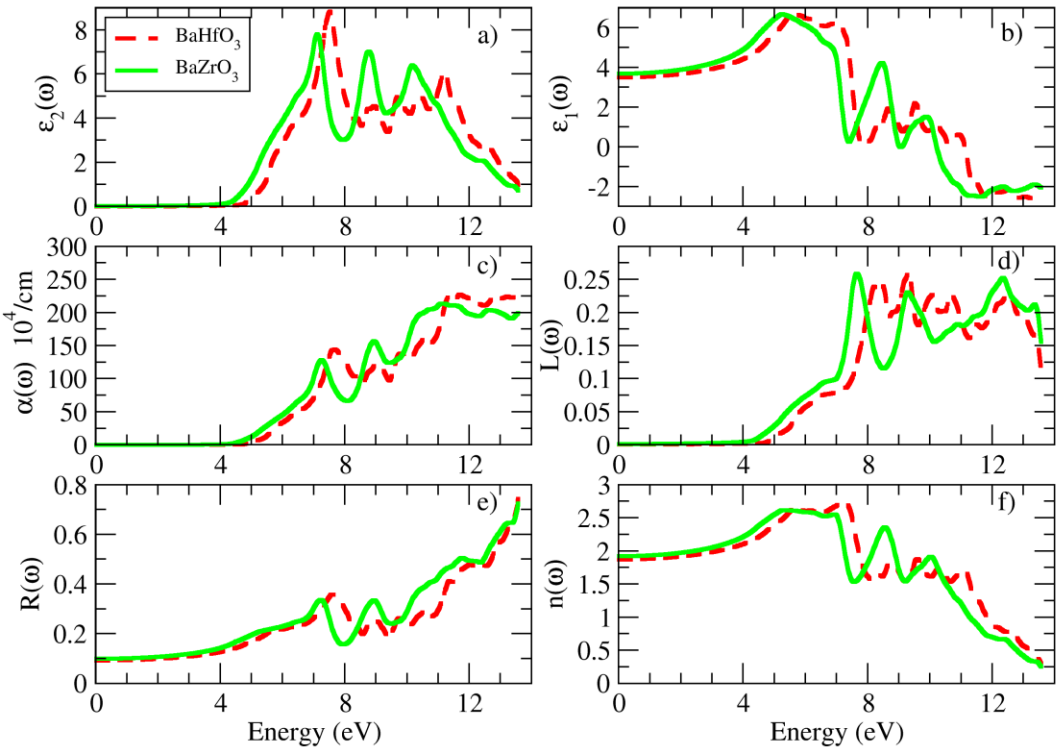
BaHfO3
BaZrO3
a)
b)
c)
d)
e)
f)
ε2(ω)
ε1(ω)
α(ω) 10^4/cm
L(ω)
R(ω)
n(ω)
Energy (eV)
Energy (eV)

Figure 6

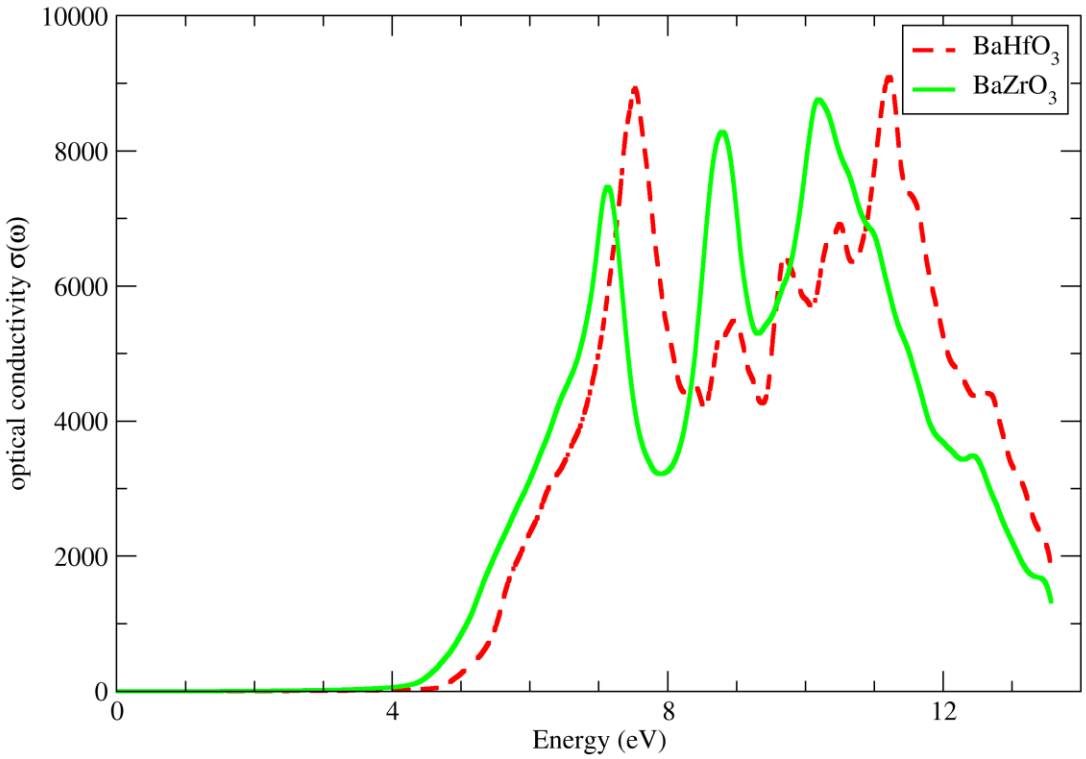
10000
8000
6000
4000
2000
0
optical conductivity σ(ω)
0
4
8
12
Energy (eV)
BaHfO3
BaZrO3

Figure 7

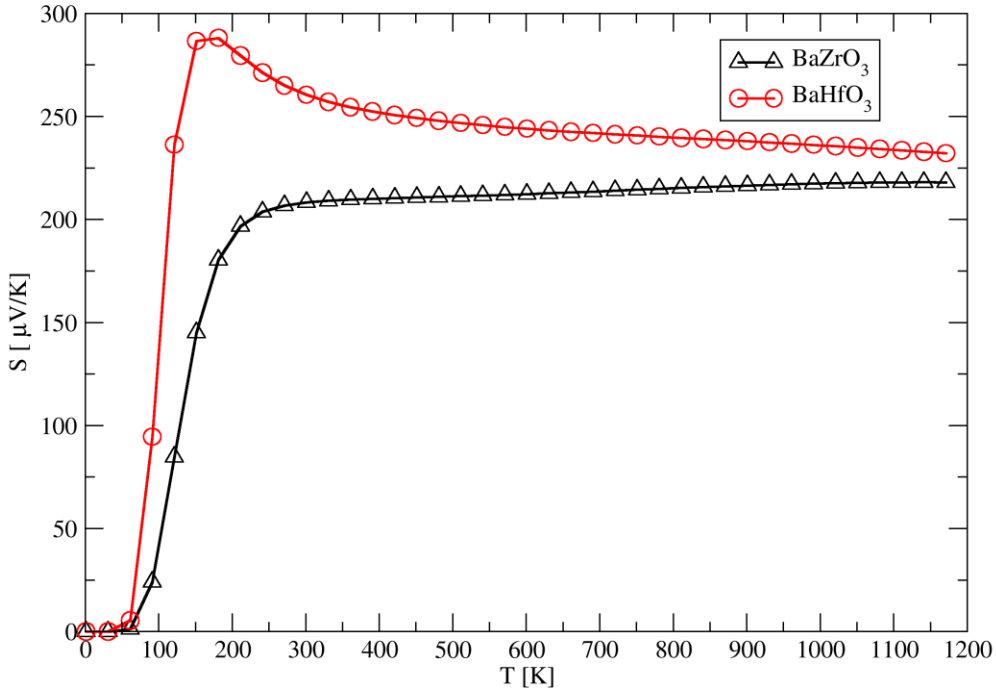
BaZrO3
BaHfO3
S [μV/K]
T [K]
0
50
100
150
200
250
300
0
100
200
300
400
500
600
700
800
900
1000
1100
1200

Figure 8

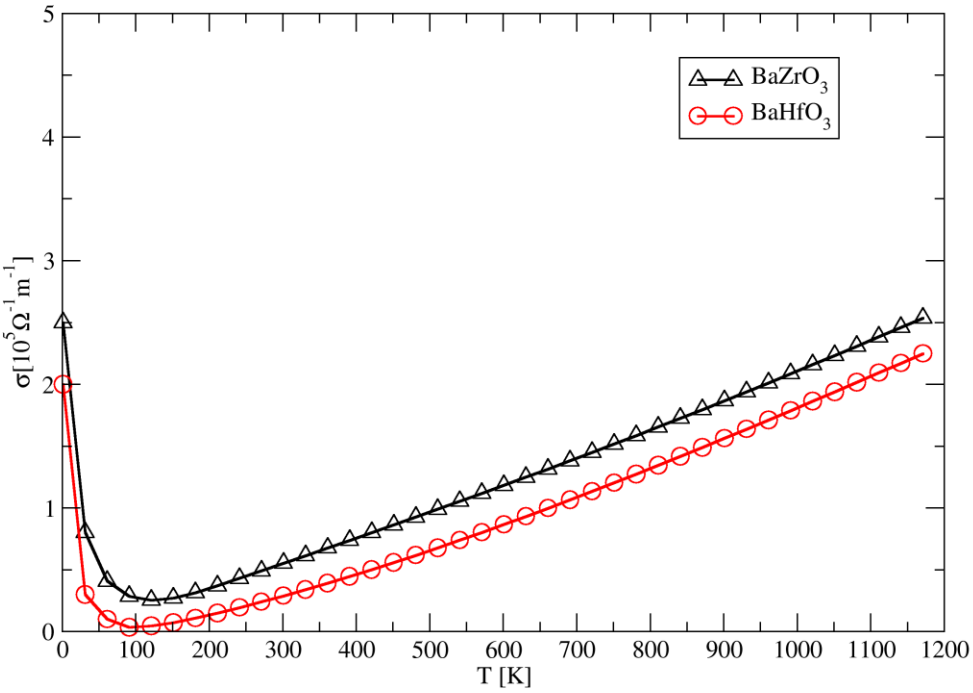
BaZrO3
BaHfO3
σ[10^5Ω^-1 m^-1]
T [K]
0
1
2
3
4
5
0
100
200
300
400
500
600
700
800
900
1000
1100
1200

Figure 9

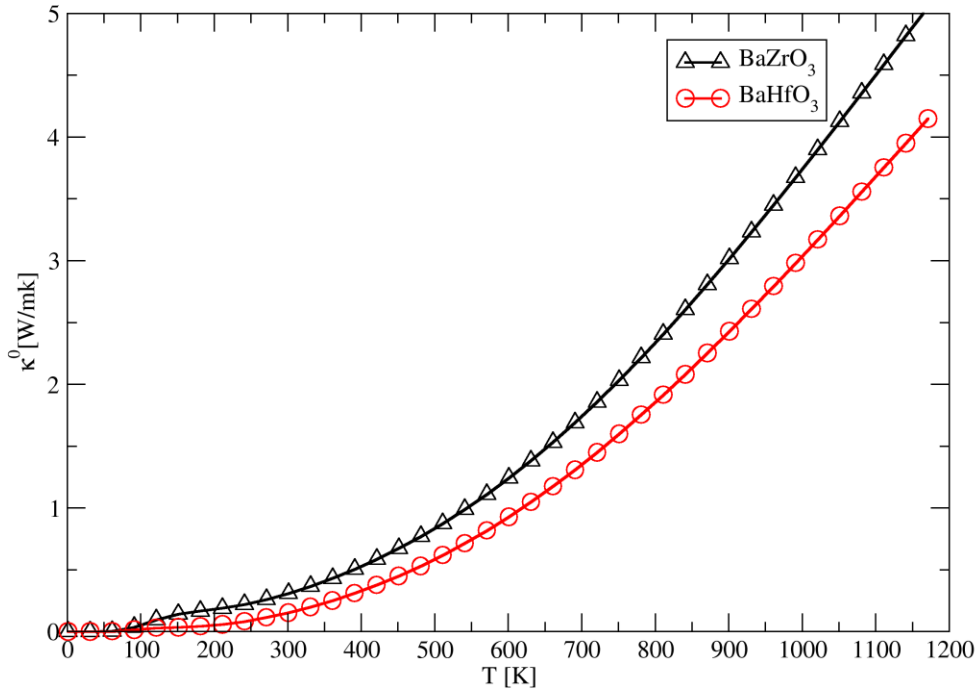
BaZrO3
BaHfO3
κ0 [W/mk]
T [K]
0
1
2
3
4
5
0
100
200
300
400
500
600
700
800
900
1000
1100
1200

Figure 10

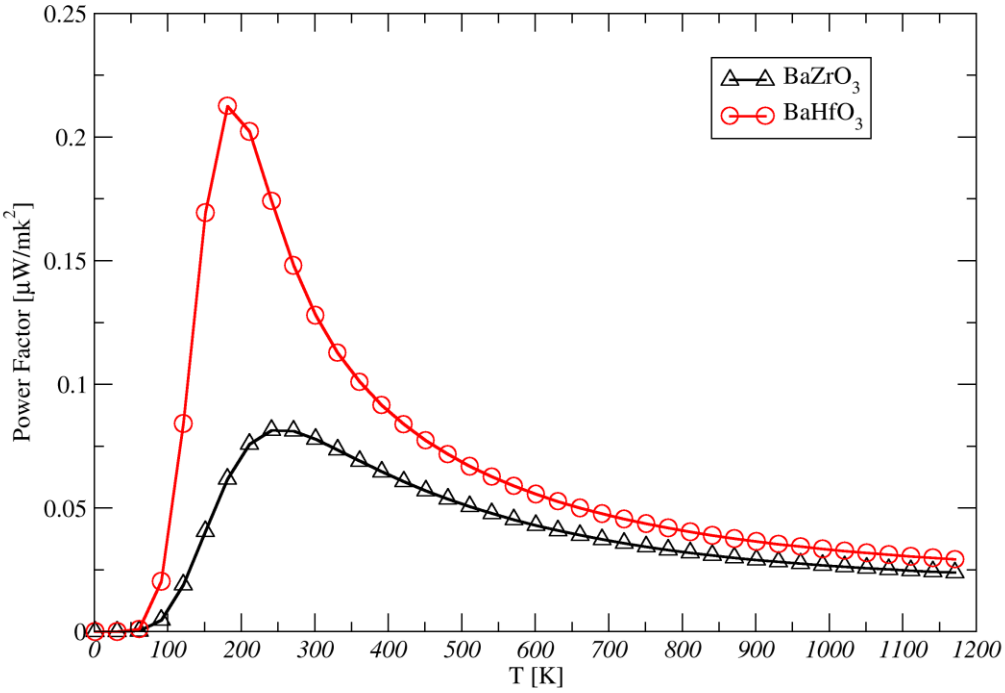
0.25
0.2
0.15
0.1
0.05
0
Power Factor [μW/mk^2]
0
100
200
300
400
500
600
700
800
900
1000
1100
1200
T [K]
BaZrO$_3$
BaHfO$_3$

Figure 11

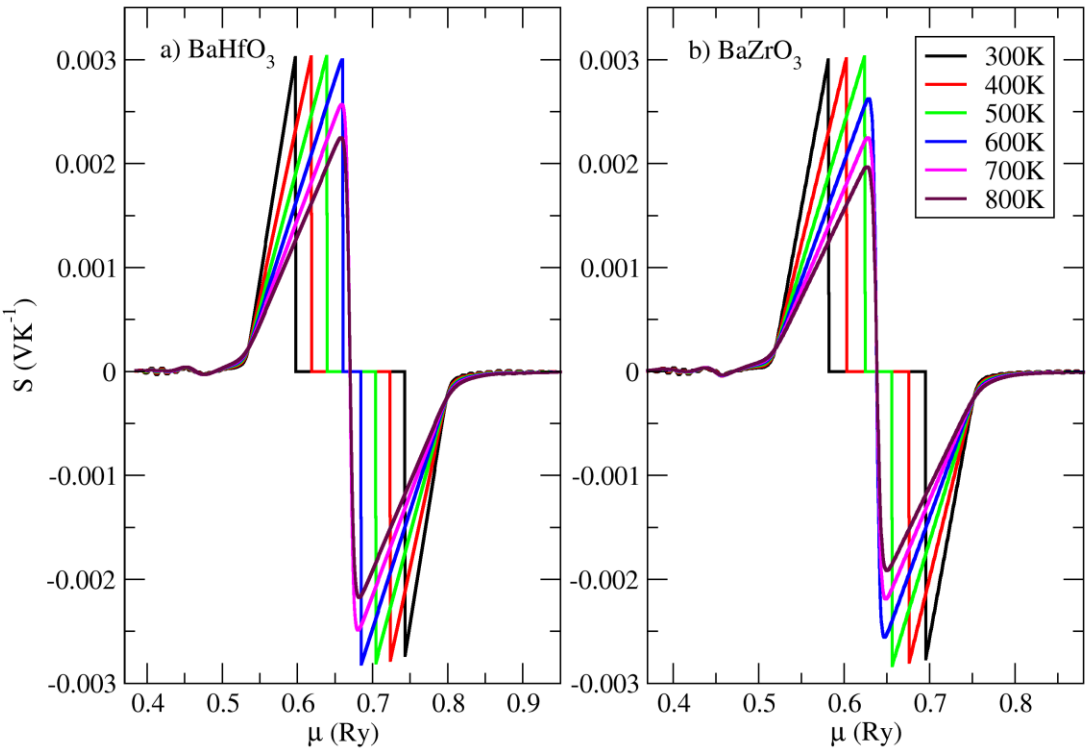
a) BaHfO3
b) BaZrO3
300K
400K
500K
600K
700K
800K
S (VK-1)
μ (Ry)
μ (Ry)
0.003
0.002
0.001
0
-0.001
-0.002
-0.003
0.4
0.5
0.6
0.7
0.8
0.9

Figure 12

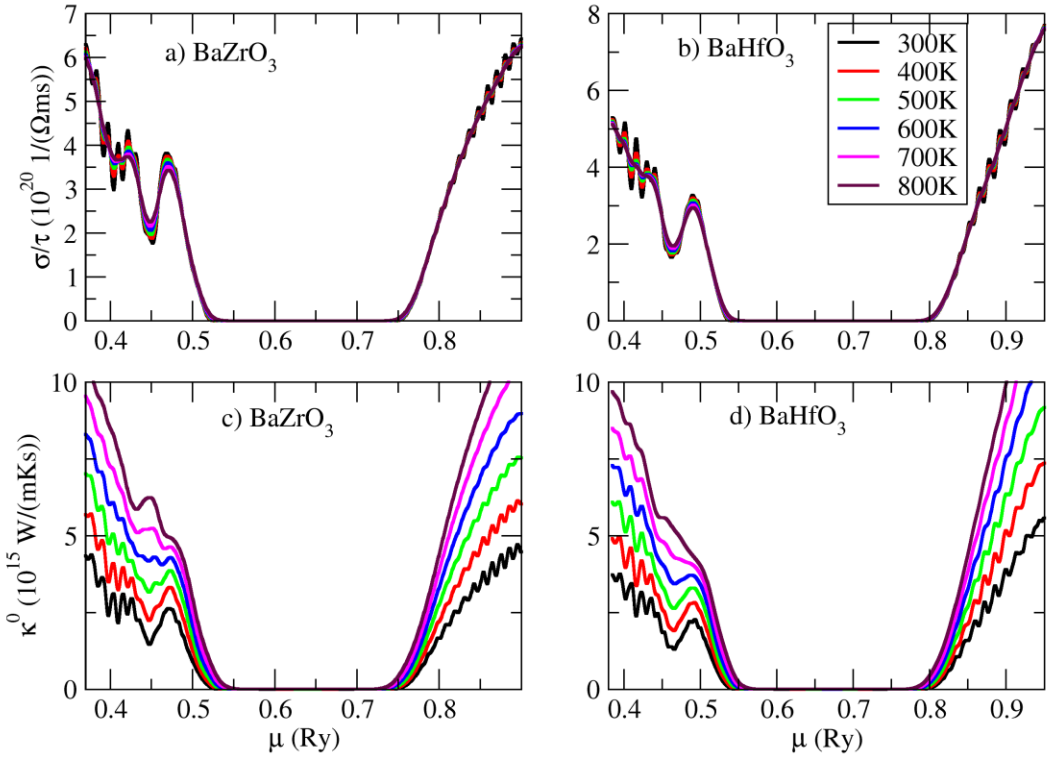
a) BaZrO3
b) BaHfO3
c) BaZrO3
d) BaHfO3
300K
400K
500K
600K
700K
800K
σ/τ (10^20 1/(Ωms))
κ0 (10^15 W/(mKs))
μ (Ry)
μ (Ry)

Figure 13

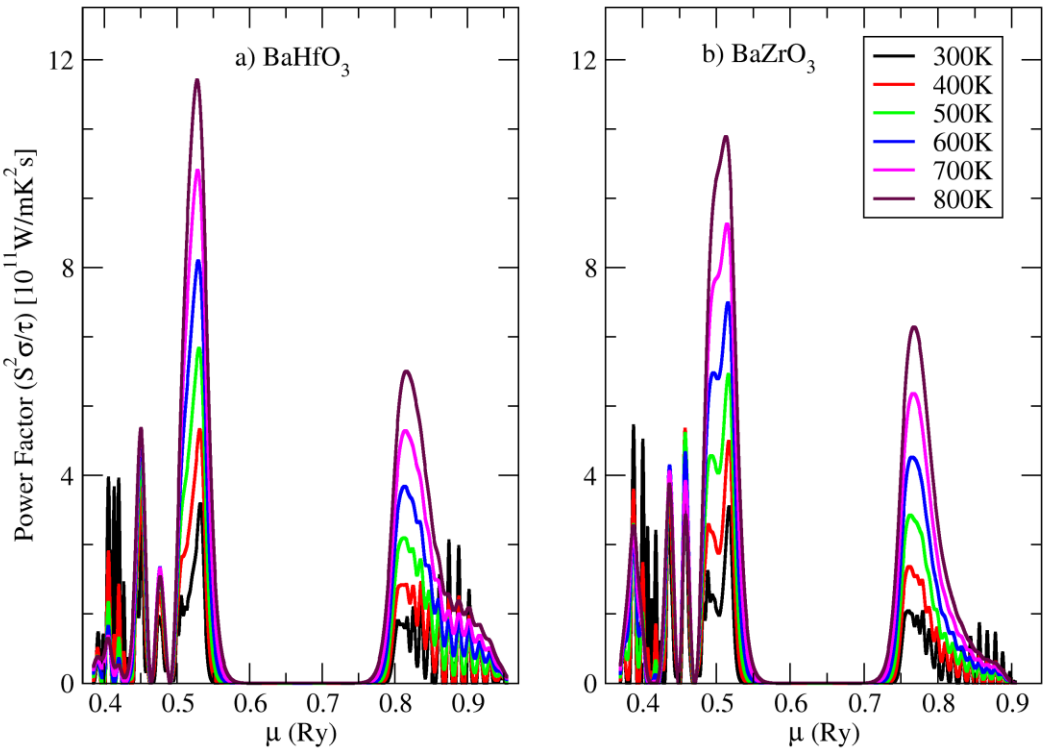
a) BaHfO3
b) BaZrO3
300K
400K
500K
600K
700K
800K
Power Factor (S2σ/τ) [10^11 W/mK2s]
μ (Ry)
μ (Ry)
0
4
8
12
0.4
0.5
0.6
0.7
0.8
0.9

Figure 14

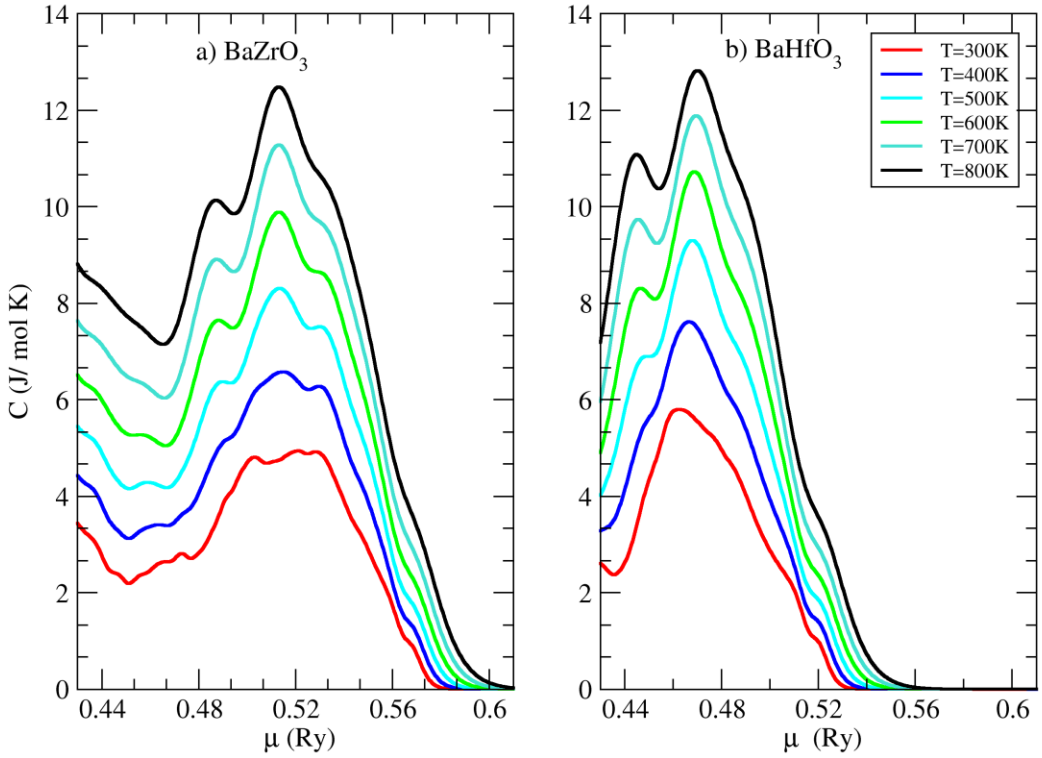
a) BaZrO3
b) BaHfO3
T=300K
T=400K
T=500K
T=600K
T=700K
T=800K
C (J/ mol K)
μ (Ry)
μ (Ry)
0
2
4
6
8
10
12
14
0.44
0.48
0.52
0.56
0.6

Figure 15

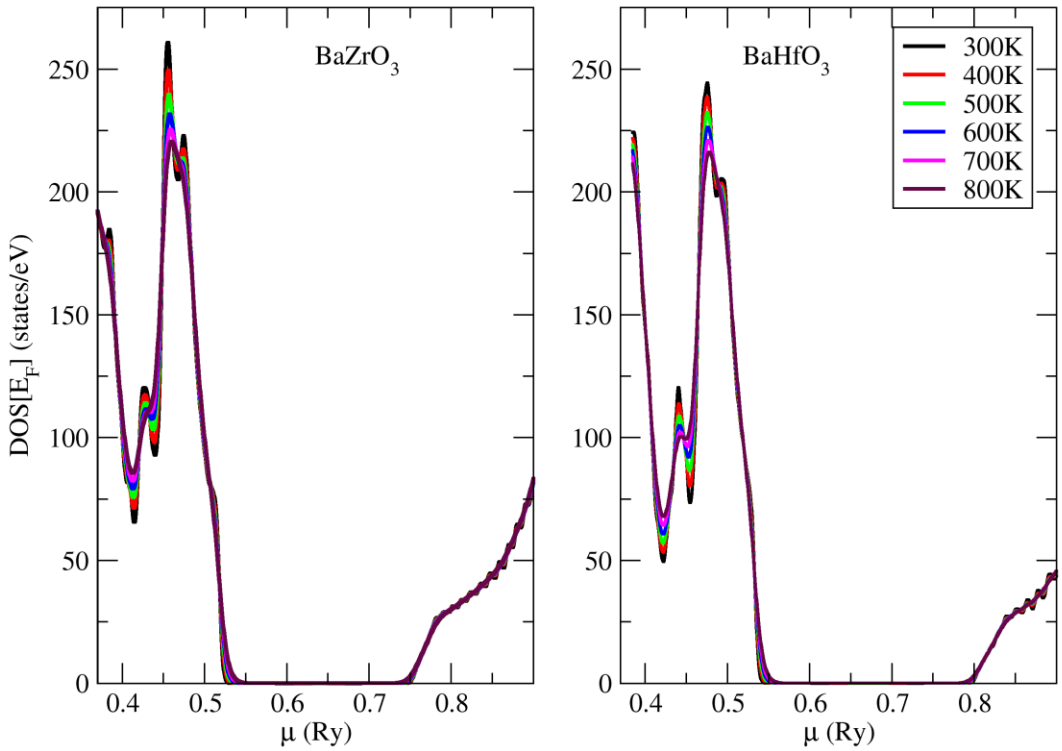
BaZrO3
BaHfO3
300K
400K
500K
600K
700K
800K
DOS[EF] (states/eV)
μ (Ry)
μ (Ry)
0
50
100
150
200
250
0.4
0.5
0.6
0.7
0.8

Figure 16

Highlights:

1- In this study, the electronic, optical and thermoelectric properties of Ba(Zr, Hf)O3 perovskites are investigated computationally using LAPW method as implemented in DFT.

2- The two compounds exhibit insulator properties with wide indirect band gap.

3- The two compounds have good optical properties that make them potential candidates for optoelectric applications.

4- The transport properties for both compounds are not as good to use in thermoelectric applications.

Credit Author Statement

- **Said Al Azar:** Conceptualization, Methodology, Software, Formal analysis
- **Ibrahim Al-Zoubi**: Data curation, Writing- Original draft preparation.
- **Ahmad Mousa**: Visualization, Software, Investigation.
- ***Riad S. Masharfe****:* Writing- Reviewing and Editing
- **Emad K. Jaradat**: Supervision Validation

,

Author declaration

1. Conflict of Interest

Potential conflict of interest exists:

We wish to draw the attention of the Editor to the following facts, which may be considered as potential conflicts of interest and to significant financial contributions to this work:

The nature of potential conflict of interest is described below:

☒No conflict of interest exists.

We wish to confirm that there are no known conflicts of interest associated with this publication and there has been no significant financial support for this work that could have influenced its outcome.

2. Funding

☒No funding was received for this work.

3. Intellectual Property

☒We confirm that we have given due consideration to the protection of intellectual property associated with this work and that there are no impediments to publication, including the timing of publication, with respect to intellectual property. In so doing we confirm that we have followed the regulations of our institutions concerning intellectual property.

4. Research Ethics

☒We further confirm that any aspect of the work covered in this manuscript that has involved human patients has been conducted with the ethical approval of all relevant bodies and that such approvals are acknowledged within the manuscript.

☒We confirm that the manuscript has been read and approved by all named authors.

☒We confirm that the order of authors listed in the manuscript has been approved by all named authors.

6. Contact with the Editorial Office

The Corresponding Author declared on the title page of the manuscript is:

Said Al Azar

☒This author submitted this manuscript using his/her account in EVISE.

☒We understand that this Corresponding Author is the sole contact for the Editorial process (including EVISE and direct communications with the office). He/she is responsible for communicating with the other authors about progress, submissions of revisions and final approval of proofs.

☒We confirm that the email address shown below is accessible by the Corresponding Author, is the address to which Corresponding Author's EVISE account is linked, and has been configured to accept email from the editorial office of American Journal of Ophthalmology Case Reports:

Q_saed74@yahoo.com

We the undersigned agree with all of the above.

	Author's name (Fist, Last)	Signature	Date
1.	____Said Al Azar_	____Sazar_____	___08 Nov 2020__
2.	___ Ibrahim Al-Zoubi _	___I. Alzoubi____	___08 Nov 2020___
3.	_____ Ahmad Mousa ___	___A. Mousa_____	__08 Nov 2020___
4.	_____ Riad Masharfe___	____R. Masharfe____	___08 Nov 2020__
5.	____ Emad K. Jaradat__	__E. Jaradat___	___08 Nov 2020_

Investigation of Electronic, Optical and Thermoelectric Properties of Perovskite $BaTMO_3$ (TM=Zr, Hf): First Principles Calculations

Said Al Azar[1*], Ibrahim Al-Zoubi[2], Ahmad A. Mousa[3], Riad S. Masharfe[4], Emad K. Jaradat[2]
[1] Research and Development Department, Ontario Academy, Amman, Jordan
[2] Department of Physics, Mutah University, Karak, Jordan
[3] Department of Basic Sciences, Middle East University, Amman, 11831, Jordan
[4] Physics Department, Zarqa University, Zarqa, Jordan

Abstract: The structural, electronic, optical, and thermoelectric characteristics of crystalline oxides-perovskites $BaTMO_3$ (TM=Zr or Hf) were investigated using the all-electron full-potential linearized augmented plane wave (FP-LAPW) method within the framework of density functional theory (DFT). The generalized gradient approximation as parameterized in Perdew, Burke, and Ernzerhof (PBE-GGA) was employed to calculate exchange-correlation potential. Also, the modified Becke Johnson exchange potential approximation as parameterized by Tarn and Blaha (TB-mBJ) was used to improve the bandgap estimation. According to our calculations, both perovskites $BaZrO_3$ and $BaHfO_3$ show insulator behavior and have widely indirect band-gap energy (R-Γ) 4.42 (3.39) eV for $BaZrO_3$ and 5.25 (3.69) eV for $BaHfO_3$ from both approaches, TB-mBJ (PBE-GGA), respectively. The optical properties such as dielectric tensor, the refractive index, the absorption coefficient, and the electron loss function have been calculated and analyzed. The optical transitions mainly take place if an electron radiate from the initial state O-2p to the final state Hf-5d or to the Zr-4d in $BaHfO_3$ or $BaZrO_3$ case, respectively. Furthermore, the transport characteristics calculations based on semi-classical Boltzmann theory have been discussed. The thermopower at RT of both compounds $BaHfO_3$ and $BaZrO_3$ are 260.47 and 208.33 μV/K, respectively. This result is good enough to consider these materials as promise thermoelectric candidates. Our results were compared with the previous ab intio calculations and experiments and showed a reasonable agreement.

Keywords: Perovskite, DFT, PBE-GGA, TB-mBJ, Optical, Ferroelectric, $BaZrO_3$, $BaHfO_3$, Thermoelectric.

*corresponding author (q_saed74@yahoo.com)

1. Introduction

Both Barium Zirconate ($BaZrO_3$) and Barium Hafnate ($BaHfO_3$) perovskites get more attention experimentally[1–6] and theoretically[7–11] because of their unique physical properties and potential applications as functional materials. They show an extensive variety and fascinating characteristics such as ferroelectricity, piezoelectricity frequency doublers, superconductivity, giant magnetoresistance, and the exchange of structural, optical, magnetic, electronic characteristics[2,12,13]. The Perovskites (ABX_3), A and B are cations and X is an anion. There are many kinds of the perovskite structure crystals, such as the oxides-perovskites (ABO_3), flouro-perovskites (ABF_3), anti-perovskite (A_3BX), double-perovskite (A_2BO_6) and nitrides-anti-perovskites (A_3BN)[14]. Furthermore, the perovskite single crystals are considered as proper candidates in solar cells, photodetectors, LED, and laser applications because of their facile fabrication and excellent optoelectronic characteristics[15].

Barium Zirconate, $BaZrO_3$ is a surface effect ceramic material that has many mechanical and technological applications[16]. Also, $BaZrO_3$ has some unique properties such as high dielectric constant (~50). In addition, it has high thermal stability and wide bandgap energy (~4 eV). These diverse properties have placed this perovskite ceramic as a useful material in applications like microwave devices, and high-temperature proton conductor for electric ceramics [3]. King-Smith and Vanderbilt calculated lattice constants, band structures, zone-center phonon frequencies, and elastic constants using the FLAPW method, with the exchange local density approximation (LDA)[7]. Barium Hafnate $BaHfO_3$, which is a compound that has high-temperature melting (2893K) and unique physical properties, has been studied in both experimental and theoretical terms including thermal expansion coefficient, heat capacity, thermal conductivity, hardness, by using the X-ray diffraction pattern, and the lattice parameter of 0.4171 nm at room temperature[17]. Also, Vali studied the properties such as the electronic band structure, phonon dispersion and dielectric constants of $BaHfO_3$ using DFT. He found that $BaHfO_3$ has an indirect bandgap between (R-Γ) points about 3.533 eV[18].

Thin films of $BaHf_{1-x}TiO_3$ were deposited using pulsed liquid injection MOCVD technique on Si (100) substrate. The roughness average value (Ra) of the film was increasing with increase x-value. Also, the $BaHf_{0.75}Ti_{0.25}O_3$ thin film showed well-behavior capacitance-voltage characteristic and its k-value is around 14[19]. Evarestov investigated the structural stability for both $BaZrO_3$ and $BaHfO_3$ perovskites using hybrid functional DFT with phonon frequency calculations. The Mulliken and Born atomic charges results have emphasized the stability of cubic and covalent bonds in both crystals[10].

Photoluminescence and photocatalytic activity of bismuth doped $BaZrO_3$ were investigated experimentally using powder X-ray diffraction (XRD), UV–VIS diffuse reflectance spectroscopy, photoluminescence (PL) spectroscopy, and photocatalytic activity. The results suggested that $BaZrO_3$:Bi could be a good candidate to be used as a visible-light activated photocatalyst under excitation wavelengths less than 800 nm[20]. Parida et al synthesized $BaZrO_3$

ceramic powder by the solid-state reaction method. Their measurement indicated that $BaZrO_3$ could be used for small dielectric resonator antenna (DRA) technology because of its low fewer microwave dielectrics materials[21]. Khan and Qureshi observed that Tantalum doped $BaZrO_3$ at Ta concentration $x = 0.04$ ($BaZr_{0.96}Ta_{0.04}O_3$) gives the highest rate of hydrogen evolution (180μmol/h) along with the surface area[22].

Zhang et al conclude that the spontaneous polarization, born effective charge and dielectric of $BaZrO_3$ is significantly sensitive to epitaxial strain and the transition from paraelectric to ferroelectric happened in both compressive and tensile strain. $BaZrO_3$ could be useful for tunable dielectric materials[23]. Chen et al synthesis $BaZrO_3$ hollow nanostructure with oxygen vacancies through one step solvothermal method using ethylenediamine (EDA) as solvent for photocatalytic hydrogen evolution from pure water. The H_2 production rate is about 15 times than that of the commercial $BaZrO_3$ (BZO-C)[24]. The $BaZrO_3$ hollow nanocrystal dopant by Fe^{+3} ions were prepared through facile solvothermal method for photocatalytic H_2 from pure water under visible light. The existence of Fe (III) ion plays a key role in broadening the optical absorption range and restricting the recombination of photo-induced carriers under visible light irradiation[7,25,26].

Although these two perovskites are studied intensively, the literature review indicates that there is a paucity of thermoelectric data and calculations. The main goal of this research study is to review and investigate in details the ferroelectric and thermoelectric properties of the cubic Barium Zirconate and Barium Hafnate perovskites to design new potential applications in ferroelectric and thermoelectric technologies.

This contribution is organized as follows: an introduction with the previous overview, the computational and theoretical framework details, the results and discussion with the comparison with previously available data, and finally the conclusions are drawn.

2. Computational Details

We have performed total energy calculations for the oxides-perovskite $BaTMO_3$, an ideal cubic structure that contains only one, composed of four atoms in its unit cell. The cations Ba are at the cube corners, 1a (0, 0, 0), while the cations TM are at the center of the cube, 1b (½, ½, ½) and oxygen atoms at the center of the cube faces forming a regular octahedron, 3c (0, ½, ½) sites of Wyckoff coordinates, as shown in Figure1. The space group for these two perovskites is Pm-3m (#221). We have used the interstitial region to express that plane waves are used approximation for the calculation of exchange-correlation energy functional, namely; generalized gradient approximation (GGA) of Perdew, Burke and Ernzerhof (PBE) parameterization[27], using modified Becke Johnson exchange potential approximation as parameterized by Tran and Blaha (TB-mBJ) to calculate the electronic band structure and density of states[28]. The TB-mBJ method was known that it provides more accurate energy band gap values than PBE-GGA method with cheap calculations cost. The first-principles calculations were performed based on (DFT) to

describe the ground state[29,30]used the method of (FP-LAPW)[31] where this is performed using the computer code in Wien2k code[32]. Also, we chose the interstitial area of the plane wave with a cutoff $K_{max} \times \ R_{MT} = \ 8$, where R_{MT} is the smallest muffin-tin radius in the unit cell, also K_{max} is the largest K vector magnitude of the interstitial plane-wave expansion of the basis set. The chosen number of k-points is (16×16×16) in codes, and which corresponds to the total number of k-points of 4096.

For the optical properties, we calculated the complex dielectric function $\varepsilon(\omega) = \varepsilon_1(\omega) + i\varepsilon_2(\omega)$, where $\varepsilon_1(\omega)$ is the real part and $\varepsilon_2(\omega)$ is the imaginary part. The real part $\varepsilon_1(\omega)$ of dielectric function $\varepsilon(\omega)$ gives from the Kramer–Kronig relationship:

$$\varepsilon_1(\omega) \ = \ 1 + \frac{2}{\pi} \ P \int_0^{\infty} \frac{\acute{\omega}\varepsilon_2(\acute{\omega})}{(\acute{\omega})^2 - \omega^2} \ d\acute{\omega} \qquad [1]$$

where the P is the principal value of the integral. The imaginary part $\varepsilon_2(\omega)$ was calculated from the momentum matrix elements between the occupied and unoccupied wave functions within the selection rules

$$\varepsilon_2(\omega) \ = \ (\frac{\hbar^2 e^2}{\pi m^2 \omega^2}) \ \sum_{c,v} \int d^3 \ k \langle ck|p^{\alpha}|vk\rangle\langle vk|p^{\beta}|ck\rangle \ \times \delta(\ \varepsilon ck - \ \varepsilon vk - \ \omega) \qquad [2]$$

where p is the momentum matrix element between states of bands α and β with crystal momentum k. c_k and v_k are the crystal wave functions corresponding to the conduction, and valance bands with crystal wave vector k. There are two contributions to ε(ω), namely; inter-band and intra-band transitions. The contribution inter-band is important only for metals, where be inter-band between valence-to-conduction absorption spectra. Whereas intra-band between valence-to-valence and conduction-to-conduction absorption. Which is describes the complete response of a material to the applied electromagnetic radiations field[33]. Then, the main optical parameters: the refractive index $n^{ii}(\omega)$, the extinction coefficient $k^{ii}(\omega)$, the absorption coefficient $\alpha^{ii}(\omega)$, optical conductivity $\sigma^{ij}(\omega)$, electron loss energy function $L^{ij}(\omega)$, and the normal incidence reflectivity $R^{ii}(\omega)$ in the crystal are given by[34,35].

$$n^{ii}(\omega) = \left[\frac{\sqrt{\varepsilon_1^{ii2}(\omega) + \varepsilon_2^{ii2}(\omega)} + \varepsilon_1^{ii}(\omega)}{2}\right]^{1/2} \qquad [3]$$

$$k^{ii}(\omega) = \left[\frac{\sqrt{\varepsilon_1^{ii2}(\omega) + \varepsilon_2^{ii2}(\omega)} - \varepsilon_1^{ii}(\omega)}{2}\right]^{1/2} \qquad [4]$$

$$\alpha^{ii}\,(\omega) = \frac{2\omega k^{ii}}{c} \qquad [5]$$

$$Re\sigma^{ij}(\omega) = \frac{\omega}{4\pi} Im\varepsilon_{ij} \qquad [6]$$

$$L^{ij}(\omega) = \sqrt{2}\omega\left[\sqrt{\varepsilon_1^{ij2}(\omega) + \varepsilon_2^{ij2}(\omega)} - \varepsilon_1^{ij}(\omega)\right]^{½} \quad [7]$$

$$\mathrm{R}^{ii}(\omega) = \frac{n^{ii}+ik^{ii}-1}{n^{ii}+ik^{ii}+1} \quad [8]$$

The transport properties are obtained from the analysis of band structure results based on Boltzmann theory method under the relaxation time approximation as implemented in BoltzTraP code[36,37]. To explore the properties of thermoelectric such as Seebeck coefficient (or coefficient of thermopower) (S), electrical conductivity (σ), specific heat (C_e), electronic thermal conductivity (κ°), and power factor rate (PF) a dense k-mesh of 25000 in the full Brillouin zone was used to guarantee good results.

The Seebeck coefficient (S) is related to carrier concentration via the Mott formula as follows[38]:

$$\mathrm{S} = \frac{\pi^2 k_B T}{3e}\left\{\frac{1}{h}\frac{dn(E)}{dE} + \frac{1}{\mu}\frac{d\mu(E)}{dE}\right\} \quad [9]$$

where e is the electron charge, k_B is Boltzmann constant, h is the Planck constant, μ is carrier mobility and n is the carrier concentration.

Electrical conductivity (σ) is related to carrier concentration as follows[39]:

$$\sigma = \frac{ne^2\tau}{m} \quad [10]$$

where m is the electron mass, n is the carrier concentration and τ is the relaxation time.

Electronic specific heat (C_e) is related to temperature and chemical potential as follows[40]:

$$\mathrm{C}_e(\mathrm{T};\ \mu) = \int n(\varepsilon)(\varepsilon-\mu)\left[\frac{df\mu(T;\varepsilon)}{dT}\right]d\varepsilon \quad [11]$$

3. **Results and Discussion**

3.1 **Structural Properties**

Goldschmidt tolerance factor (t) for perovskite is given by[41]:

$$t = \frac{(r_A+r_X)}{\sqrt{2}(r_B+r_X)} \quad [12]$$

Where $r_N$is the ionic radius of atom N. The t values of existence perovskite compounds range is ($0.75 < t \leq 1$). For ideal cubic perovskite structure, t has unity value. The tolerance factor t for $BaZrO_3$ and $BaHfO_3$ are 1.0 and 1.016, respectively.

We presented the relationship between the energy changes as a function of the unit cell volume. Using the Birch-Murnaghan equation of state to determine the different important structural and ground-state properties[42]. The equilibrium lattice constants (α) and ground-state energies (E_0) are calculated, as estimated from optimization at zero pressure. Besides the volume, the lattice constants increase because of the increase in the atomic radius from Zr to Hf. In the present work, we were fitting the energy-volume values to a third-order Birch-Murnaghan equation of state to calculate lattice parameter α and bulk modulus B_0 of Ba(Zr, Hf)O_3 compounds, where the bulk modulus increases as the volume decreasing with moving of cation down in the group in the periodic table. The calculated ground-state parameters for both $BaZrO_3$ and $BaHfO_3$ are tabulated in Table 1 along with previous computational and experimental studies. For both perovskites, our results are in reasonable agreement with the available experimental data and previous calculations.

3.2 Electronic properties

To study the electronic properties of $BaZrO_3$ and $BaHfO_3$, DOS's and band structures along the symmetry direction of the first Brillouin zone, of these compounds both PBE-GGA, and TB-mBJ methods for exchange-correlation potential are used. The band structures for $BaZrO_3$ and $BaHfO_3$ are presented in figure 2. The Fermi level E_F is chosen to locate at 0 eV. In both methods, the $BaZrO_3$ shows semiconductor characteristics with indirect bandgap (E_g) ($R \rightarrow \Gamma$), but in the TB-mBJ method, the (E_g) is wider. The valence band maximum (VBM) occurs along the R-point symmetry line, while the conduction band minimum (CBM) occurs along the Γ-point symmetry line. The bandgap approaches 3.39 eV by using the PBE-GGA method whereas it approaches 4.424 eV by using the TB-mBJ method. As well, $BaHfO_3$ shows the same behavior with indirect semiconductor bandgap ($R \rightarrow \Gamma$), where the bandgap is 3.69 eV by using the PBE-GGA method and 5.246 eV when using the TB-mBJ method. Table 2, the calculated bandgap (E_g) of both perovskites $BaZrO_3$ and $BaHfO_3$ are compared with previous theoretical and experimental data. For both compounds, the TB-mBJ values approach enough to experimental results.

The total density of state (TDOS) and partial density of state (PDOS) site projected for both compounds are calculated using both methods PBE-GGA and TB-mBJ. The TDOS and PDOS for $BaZrO_3$ are shown in figure 3a. It is clear that the lower valence band consist of Ba-*p* state around -10.1 to -11 eV, and the upper valence band extends down to approximately -4 eV and is composed mainly of O-*p* states with a small contribution from Zr-*d* states, while the lower conduction band is mainly a mixture of Ba-*d* and Zr-*d* states, with a small admixture from O-*p*. In the conduction bands, the Zr-*d* states are dominant. Figure 3b displays the TDOS and PDOS for $BaHfO_3$ perovskite using both PBE-GGA and TB-mBJ methods. The contribution to the lowest valence band at −10 eV is due to Ba-*p* state, whereas the upper valence band (around -4.2 to 0 eV) is from O-*p* states hybridized with some Hf-*p* and Hf-*d* electrons. These O-*p* and Hf-*d* hybridizations suggest covalent bonding contributions. The bands above the Fermi level are the

conduction band of the compound; the lower part of the band (around 3.8 to 6 eV) is dominated by the O-*p*. Also, it can be seen from the plot that the top of conduction bands consist mainly Ba-*d* and Hf-*d* states hybridized with some O-*p*. The conduction bands are composed mostly of antibonding between Hf-*d* and O-*p* as well as antibonding between Ba-*d* and O-*p*, maximum peak at 7.5 eV is due to the unoccupied 5*d* states of Hf (*5d-eg*) antibonding with O-*2p* mixed with Ba-*5d* and O-*2p*.

3.3 Optical Properties

In this subsection, the optical characteristics of $BaHfO_3$ and $BaZrO_3$ are presented. Electronic excitations will take place within the crystal if it is exposed to electromagnetic radiation. As a result, the optical features of the crystal will be observed. The nature of the response to an incident electromagnetic wave at a particular frequency determines if this material could be used in optoelectronic devices. The different optical characteristics of the crystals are mainly calculated by using the frequency-dependent complex dielectric tensor $\varepsilon^{ij}(\omega)$. Since $BaZrO_3$ and $BaHfO_3$ perovskites has cubic structure symmetry which means one tensor component is enough to do optical calculations. Thus, the optical characteristics of the materials $n(\omega)$, $k(\omega)$, $R(\omega)$, $\sigma(\omega)$, $\alpha(\omega)$, and $L(\omega)$ could be derived from their $\varepsilon_1(\omega)$ and $\varepsilon_2(\omega)$ values as illustrated in the computational details section[43].

The imaginary part $\varepsilon_2(\omega)$ is determined from the electronic structure through the joint density of states and the momentum matrix elements between the occupied and the unoccupied wave functions within the selection rules. In figure 4, the optical characteristics for both $BaZrO_3$ and $BaHfO_3$ compounds are plotted. In panel a) the spectrum of $\varepsilon_2(\omega)$ shows the three peaks structure for $BaZrO_3$ and $BaHfO_3$. The $\varepsilon_2(\omega)$ has deeply impact on the absorption spectrum of the matter. A large value of $\varepsilon_2(\omega)$ refers to a large absorption spectrum include of the whole of all different transitions that will occur between the valance and the conduction bands. It is starting to response to the incident radiation at critical points which are the threshold energy at 2.87 eV and 4.26 eV for $BaZrO_3$ and $BaHfO_3$ respectively. These points are C_v–C_c splitting and give a threshold for indirect optical transitions between the highest valance band and the lowest conduction band. This is known as the fundamental absorption edge. The main peak in the spectrum is situated at 7.12 eV and 7.52 eV for $BaZrO_3$, and $BaHfO_3$, respectively. These peaks are dominated by transitions from the O-*p* band and the small contribution of transition metals *d* state just below Fermi energy to Ba-*p* state of the conduction band. In panel b) the spectrum of $\varepsilon_1(\omega)$ for $BaZrO_3$ and $BaHfO_3$ compounds show that the static dielectric constant $\varepsilon_1(0)$ are equal 3.69 and 3.51, whereas the main peaks appear at energy 5.24 eV and 5.59 eV, respectively. It is important to consider both ε_1 and ε_2 together since they affect each other, meaning the shape of ε_2 cause corresponding changes in the shape of ε_1 and vice-versa. This is known as the Kramers-Kronig relation between the real (ε_1) and imaginary (ε_2) parts of the dielectric function. In short, the dielectric function describes what an electric field such as an oscillating light wave does to the material. In panel c) the absorption coefficients for $BaZrO_3$ and $BaHfO_3$ compounds show the same behavior as $\varepsilon_2(\omega)$. The absorption edges start from 3.28 and 4.29 eV for $BaZrO_3$ and $BaHfO_3$ respectively which are corresponding to optical bandgaps. This produces from the transition of the O-p valence band electrons to the empty d conduction bands in Zr or Hf. In $BaHrO_3$ perovskite, the main peak in dielectric absorption spectra occurs at 7.81 eV whereas the two other peaks at 11.3 and 11.78 eV whereas in $BaZrO_3$ the main peak occurs at 7.31 eV the

other two peaks occur at 8.8 and 11.0 eV. In both compounds, the Ba does not contribute to the low-energy absorption spectra; because its electron valence bands are not in the transition energy domain. In panel d) the loss function for $BaZrO_3$ and $BaHfO_3$ compounds are plotted and their peaks occur at 7.6 eV and 8.4 eV, respectively. In panel e) the reflectivity for both $BaZrO_3$ and $BaHfO_3$ compounds are plotted and their static reflectivity $R(0)$ is approximately equal 10%. At low energies (i.e., 0–7.8 eV for $BaHfO_3$ and 0–7.2 eV for $BaZrO_3$), the reflectivity spectrum was observed to extend as high as 33% and 30% for $BaHfO_3$ and $BaZrO_3$, respectively. Our calculations show a strong reflectivity at high energies increase up to 75%, and 72% for $BaHfO_3$, and $BaZrO_3$, respectively. In panel f) the refractive index plots show that the static refractive index $n(0)$ are equal 1.92 and 1.87 for $BaZrO_3$ and $BaHfO_3$, respectively. The refractive index reaches its maximum value 2.7 at 7.5 eV for $BaHfO_3$, whereas for $BaZrO_3$ its 2.5 occurs at 5.0 eV. Finally, the optical conductivity $\sigma(\omega)$ for both $BaZrO_3$ and $BaHfO_3$ perovskites are displayed in panel g). There is quite similarity in curves of both perovskites. For $BaZrO_3$ the first peak appears at 6.8 eV, the second peak appears at 9.0 eV whereas the third peak at 10.5 eV. On the other hand, at $BaHfO_3$ there are two mean peaks at 7.4 eV and 11.5 eV. The maximum value for $BaZrO_3$ is equal 8900 at 10.5 eV while for $BaHfO_3$ it is equal 9100 at 11.5 eV.

3.4 Thermoelectric (TE) Properties

The efficient thermoelectric characteristics for any materials determines by their figure of merit $zT = S^2\sigma T/\kappa$, the increasing of S and σ increase figure of merit while increasing the total thermal conductivity κ decrease figure of merit. As it is known, a suitable material for thermoelectric applications should have figure of merit equal or greater than one which give energy transformation efficiency greater than 25% at optimal operating temperature[44].

Figure 5a shows the variation of Seebeck coefficient S with respect to temperature for both compounds $BaZrO_3$ and $BaHfO_3$. The two curves have approximately the same behavior where they change nonlinearly by increasing from zero to reach the maximum value 206.86 μV/K at T=270K for $BaZrO_3$ and 288.13 μV/K at T=180K for $BaHfO_3$, after that it is decreasing slightly in $BaHfO_3$ but in $BaZrO_3$ it is still increasing. The anomalies behavior of the Seebeck coefficient at the low temperature is due to the strong electron-phonon coupling, where the phonon drag effect becomes manifest. The peak in the Seebeck curve around 100 K in the figure is coming from the phonon drag effect. It is roughly consistent with the estimated value of $\theta_D/5$, where θ_D being the Debye temperature of both compounds [$\theta_D(BaZrO_3)$ = 544 K and θ_D ($BaHfO_3$) = 465 K]. At room temperature (RT), Seebeck coefficients for $BaZrO_3$ and $BaHfO_3$ are 208 and 261 μV/K, respectively, which are close to conventional thermoelectric material values. The positive value of S in the given temperature range defines the majority charge carriers as holes i.e. p-type semiconductors. High S implies the large effective mass due to the existence of energy bands near the Fermi level in this material. In figure 5b, the electric conductivity σ as a function of temperature when the constant relaxation time $\tau_0 = 0.8 \times 10^{-14}s$ is used, it is shown that the electric conductivity is decreasing non-linearly at the low temperature to reach its global minimum at T=121K in $BaZrO_3$ case and T=90 in $BaHfO_3$, then it starts increasing linearly with temperature increases for both $BaZrO_3$ and $BaHfO_3$. The electric conductivity at RT for $BaZrO_3$

is about $0.554 \times 10^5 S/m$ and it about $0.289 \times 10^5 S/m$ for $BaHfO_3$. Figure 5c displays the electronic thermal conductivity κ^0 as a function of temperature when the constant relaxation time $\tau_0 = 0.8 \times 10^{-14} s$ is used. The behavior of the electronic thermal conductivity curves are nonlinear increasing for both compounds. The electronic thermal conductivity of $BaHfO_3$ at RT is equal to 0.154 $Wm^{-1}K^{-1}$, which is about half the $BaZrO_3$ value of 0.309 $Wm^{-1}K^{-1}$. Our results contradict the previous experimental values 10.4[45] and 5.2[46] $Wm^{-1}K^{-1}$, respectively. This contradiction could be because our calculations are based on Boltzmann transport theory which unfortunately calculates only the electronic part (κ^0) of total thermal conductivity ($\kappa = \kappa^0 + \kappa_L$), whereas, the experimental results measured the total thermal conductivity (κ), where the lattice part (κ_L) contributed as the dominant part in both compounds. The ratio between electronic thermal conductivity and electronic conductivity obey Wiedemann-Franz law ($\frac{\kappa^0}{\sigma} = LT$), where L is the Lorentz number (in order of $\sim 10^{-8} W\Omega K^{-2}$ W) for both compounds. The temperature dependence of the thermal conductivities of $BaZrO_3$ and $BaHfO_3$ follow an inverse temperature law (1/T) at low temperatures, showing typical phonon conduction characteristics [46]. Figure 5c shows how are the power factor (PF) curves changed when the temperature increase for both compounds. They reach their maximum values 0.213 μW/mk^2 at T=180K for $BaHfO_3$ and 0.0814 μW/mk^2 at T=240K for $BaZrO_3$. Also, at RT the PF's equal 0.128 μW/mk^2 for $BaHfO_3$ and 0.0778 μW/mk^2 for $BaZrO_3$. Although the PF values for both compounds are small compared with the well-known thermoelectric materials, these results support that $BaHfO_3$ is better than $BaZrO_3$ if a suitable element dopant in specific concentrations is used and/or through band engineering or switching to nanostructures. It is possible to fabricate perovskite at the nanoscale as the lattice thermal conductivity decreases. This will improve the merit figure at room temperature; consequently, the thermoelectric efficiency increases.

To determine in details thermoelectric (TE) behavior for both $BaHfO_3$and $BaZrO_3$, such as Seebeck coefficient (S), electrical conductivity (σ), power factor (PF), electronic specific heat (C_e), and electronic thermal conductivity (κ°) have been expressed as a function of chemical energy (μ); the calculated characteristics were plotted for considered temperatures range: 300-800 K. In figure 6, S for both $BaZrO_3$ and $BaHfO_3$ compounds as a function of chemical energy μ at different temperature are plotted. For both compounds, the curve increases linearly from zero value to reach the maximum value and then decreases sharply to negative global minimum values; after that it increases linearly again to reach zero value.

The chemical potential dependencies of electric conductivity rate (σ/τ) for both $BaZrO_3$ and $BaHfO_3$ compounds at different temperatures are depicted in figure 7 panels a) and b). In the two panels, the electric conductivity goes to zero in energy range 0.52 – 0.74 Ry for $BaZrO_3$ and 0.54 – 0.8 Ry for $BaHfO_3$ for the wide range of temperatures from 200K to 800K. In figure 8 the power factor with respect to chemical energy at different temperatures is plotted; a) $BaZrO_3$ and b) $BaHfO_3$ perovskites. The two plots (a and b) display two main peaks one for n-type and the other for p -type. The p-type of $BaZrO_3$ exhibits the PF peak 11.7 $\times 10^{11}$ W/mK^{2}s at 0.525 Ry,

while the n-type 6.0 $\times 10^{11}$ W/mK^{2}s at 0.83 Ry. For $BaHfO_3$, the p-type and n-type PF peaks 10.65 $\times 10^{11}$ W/mK^{2}s and 6.75 $\times 10^{11}$ W/mK^{2}s are at 0.5 Ry and 0.775 Ry, respectively. Therefore, these materials may be used as p-type thermoelectric materials. Also, the PF values of the two compounds around E_F are negligible $PF(\mu = E_F) = 0eV$. This means that their thermoelectric properties are not good without doping. Figure 9 shows the electronic specific heat capacity as a function of chemical energy at different temperature. The calculated specific heat capacity of $BaZrO_3$ in this study is well agreement with the data in the literature[47]. The C_e values for $BaHfO_3$ are slightly greater than that of $BaZrO_3$ because of the higher molar mass of Hf compare to Zr. Figure 10 shows the variation of the density of state around the Fermi level with respect of temperature. For the two alloys $BaZrO_3$ and $BaHfO_3$ the band gap still appear for a wide range of temperature.

4. Conclusions

Employing the all-electron full-potential LAPW method based on DFT, with using PBE-GGA functional of exchange-correlation energy; and semi-local exchange potential TB-mBJ to study physical properties of both $BaZrO_3$ and $BaHfO_3$ perovskites. Also, semi-classical Boltzmann transport theory has been used to calculate the thermoelectric properties. A summary of results are:

(i) The calculated lattice constants at zero pressure of these compounds are in a reasonable agreement with the previous theoretical and experimental values.

(ii) The electronic bandstructure calculations showed that $BaZrO_3$ and $BaHfO_3$ are insulators materials with an indirect bandgap ($R-\Gamma$). The fundamental bandgap of this compounds increases when mBJ-GGA approach is used instead of PBE-GGA.

(iii) The joint DOS and the Kramers-kronig transformation are used to calculate and analyze the optical characteristics: dielectric constant $\varepsilon(\omega)$, the absorption coefficient $\alpha(\omega)$, the reflectivity $R(\omega)$, the refractive index $n(\omega)$ and electron loss energy $L(\omega)$. The oxygen p states and Transition metals Zr- and Hf-d states play a major role in optical transitions.

(iv) Finally, the calculated transport characteristics showed that the two compounds are not suitable choice for thermoelectric applications but if they are dopant with some impurities their thermoelectric properties could be improved.

References

1. Tian, H. Y. *et al.* Synthesis of $BaZr_{0.75}Hf_{0.25}O_3$ by a solid-state reaction technique and characterizations of dielectric properties. *J. Alloys Compd.* **402**, 251–255 (2005).

2. Bandura, A. V, Evarestov, R. A. & Kuruch, D. D. Hybrid HF-DFT modeling of monolayer water adsorption on (001) surface of cubic $BaHfO_3$ and $BaZrO_3$ crystals. *Surf. Sci.* **604**, 1591–1597 (2010).

3. H. Stetson & B. Schwartz. Dielectric Properties of Zirconates. *Joutnal Am. Ceram. Soc.*

44, 420 (1961).

4. Zhang, J. L. & Evetts, J. E. $BaZrO_3$ and $BaHfO_3$: preparation, properties and compatibility with YBa2Cu3O7-x. *J. Mater. Sci.* **29**, 778 (1994).

5. Megaw, H. D. Crystal structure of double oxides of the perovskite type. *Proc. Phys. Soc.* **58**, 133–152 (1946).

6. Scholder, R., Rade, D. & Schwarz, H. Uber Zirkonate, Hafnate und Thorate von Barium, Strontium, Lithium und Natrium. *Zeitschrift Anorg. und Allg. Chemie* **362**, 149–168 (1968).

7. King-Smith', R. D. & Vanderbilt, D. First-principles investigation of ferroelectricity in perovskite compounds. *Phys. Rev. B* **49**, 5828 (1994).

8. Iles, N. *et al.* Atomistic study of structural, elastic, electronic and thermal properties of perovskites $Ba(Ti,Zr,Nb)O_3$. *Comput. Mater. Sci.* **39**, 896–902 (2007).

9. Bouhemadou, A., Djabi, F. & Khenata, R. First principles study of structural, elastic, electronic and optical properties of the cubic perovskite $BaHfO_3$. *Phys. Lett. Sect. A Gen. At. Solid State Phys.* **372**, 4527–4531 (2008).

10. Evarestov, R. A. Hybrid density functional theory LCAO calculations on phonons in $Ba(Ti,Zr,Hf)O_3$. *Phys. Rev. B - Condens. Matter Mater. Phys.* **83**, 014105 (2011).

11. Verma, A. S. & Kumar, A. Bulk modulus of cubic perovskites. *J. Alloys Compd.* **541**, 210–214 (2012).

12. Zhao, H., Chang, A. & Wang, Y. Structural, elastic, and electronic properties of cubic perovskite $BaHfO_3$ obtained from first principles. *Phys. B Condens. Matter* **404**, 2192–2196 (2009).

13. Ali, Z., Khan, I., Ahmad, I., Khan, M. S. & Asadabadi, S. J. Theoretical studies of the paramagnetic perovskites $MTaO_3$ (M = Ca, Sr and Ba). *Mater. Chem. Phys.* **162**, 308–315 (2015).

14. Mubarak, A. A. & Mousa, A. A. The electronic and optical properties of the fluoroperovskite $BaXF_3$ (X = Li, Na, K, and Rb) compounds. *Comput. Mater. Sci.* **59**, 6–13 (2012).

15. Rong, S.-S., Faheem, M. B. & Li, Y.-B. Perovskite single crystals: Synthesis, properties, and applications. *J. Electron. Sci. Technol.* 100081 (2021) doi:10.1016/j.jnlest.2021.100081.

16. Nakashima, K. *et al.* Preparation of $BaZrO_3$ nanoparticles using a solvothermal reaction. in *IOP Conference Series: Materials Science and Engineering* vol. 18 (Institute of Physics Publishing, 2011).

17. Khenata, R. *et al.* First-principle calculations of structural, electronic and optical properties of $BaTiO_3$ and $BaZrO_3$ under hydrostatic pressure. *Solid State Commun.* **136**,

120–125 (2005).

18. Vali, R. Lattice dynamics and electronic properties of the scintillator host material: Barium hafnate. *Solid State Commun.* **147**, 1–3 (2008).

19. Abrutis, A. *et al.* Chemical vapor deposition and characterization of high-k $BaHf_{1-x}Ti_xO_3$ dielectric layers for microelectronic applications. *J. Vac. Sci. Technol. B, Nanotechnol. Microelectron. Mater. Process. Meas. Phenom.* **29**, 01A303 (2011).

20. Borja-Urby, R. *et al.* Structural study, photoluminescence, and photocatalytic activity of semiconducting $BaZrO_3$:Bi nanocrystals. in *Materials Science and Engineering B: Solid-State Materials for Advanced Technology* vol. 176 1382–1387 (2011).

21. Parida, S. *et al.* Structural refinement, optical and microwave dielectric properties of BaZrO3. *Ceram. Int.* **38**, 2129–2138 (2012).

22. Khan, Z. & Qureshi, M. Tantalum doped $BaZrO_3$ for efficient photocatalytic hydrogen generation by water splitting. *Catal. Commun.* **28**, 82–85 (2012).

23. Zhang, Y., Liu, M., Wang, J., Shimada, T. & Kitamura, T. Strain tunable ferroelectric and dielectric properties of $BaZrO_3$. *J. Appl. Phys.* **115**, 224107 (2014).

24. Chen, T. *et al.* One-step synthesis of hollow $BaZrO_3$ nanocrystals with oxygen vacancies for photocatalytic hydrogen evolution from pure water. *J. Alloys Compd.* **780**, 498–503 (2019).

25. Meng, J. *et al.* $BaZrO_3$ hollow nanostructure with Fe (III) doping for photocatalytic hydrogen evolution under visible light. *Int. J. Hydrogen Energy* **43**, 9224–9232 (2018).

26. Khirade, P. P., Birajdar, S. D., Shinde, A. B. & Jadhav, K. M. Room temperature ferromagnetism and photoluminescence of multifunctional Fe doped $BaZrO_3$ nanoceramics. *J. Alloys Compd.* **691**, 287–298 (2017).

27. Perdew, J. P., Burke, K. & Ernzerhof, M. Generalized Gradient Approximation Made Simple. *Phys. Rev. Lett.* **77**, 3865 (1996).

28. Tran, F. & Blaha, P. Accurate band gaps of semiconductors and insulators with a semilocal exchange-correlation potential. *Phys. Rev. Lett.* **102**, 226401 (2009).

29. Hohenberg, P. & Kohn, W. Inhomogeneous Electron Gas. *Phys. Rev.* **136**, B864–B871 (1964).

30. Kohn, W. Density Functional and Density Matrix Method Scaling Linearly with the Number of Atoms. *Phys. Rev. Lett.* **76**, 3168 (1996).

31. Singh, D. J. & Nordström, L. *Planewaves, pseudopotentials and the LAPW method*. (Springer Science & Business Media, 2006).

32. Blaha, P. *et al.* WIEN2k: An APW+lo program for calculating the properties of solids. *J. Chem. Phys.* **152**, 074101 (2020).

33. Smith, N. V. Photoelectron Energy Spectra and the Band Structures of the Noble Metals. *Phys. Rev. B* **3**, 1862–1878 (1971).

34. Mark Fox. *Optical Properties of Solids*. (Oxford University Press, 2010).

35. M. Dreesel & G. Gruner. *Electrodynamics of Solids: Optical Properties of Electrons in Matter*. (Cambridge University Press, 2002).

36. Madsen, G. K. H. & Singh, D. J. BoltzTraP. A code for calculating band-structure dependent quantities. *Comput. Phys. Commun.* **175**, 67–71 (2006).

37. Khandy, S. A. & Gupta, D. C. Investigation of structural, magneto-electronic, and thermoelectric response of ductile $SnAlO_3$ from high-throughput DFT calculations. *Int. J. Quantum Chem.* **117**, e25351 (2017).

38. Cutler, M. & Mott, N. F. Observation of anderson localization in an electron gas. *Phys. Rev.* **181**, 1336–1340 (1969).

39. P Drude. Zur Elektronentheorie der Metalle. *Ann. Phys.* **306**, 566 (1900).

40. Ashcroft, N. W. & Mermin, N. D. *Solid state physics*. (Philadelphia, saunders college, 1976).

41. Bhalla, A. S., Guo, R. & Roy, R. The perovskite structure—a review of its role in ceramic science and technology. *Mater. Res. Innov.* **4**, 3–26 (2000).

42. Birch, F. Elasticity And Constitution Of The Earth's Interior. *J. Geophys. Res.* **57**, 60 (1952).

43. Chanda, S. *et al.* Calculations of the structural and optoelectronic properties of cubic $Cd_xZn_{1-x}Se_yTe_{1-y}$ semiconductor quaternary alloys using the DFT-based FP-LAPW approach. *J. Comput. Electron.* **19**, (2020).

44. Alrahamneh, M. J., Mousa, A. A. & Khalifeh, J. M. First principles study of the structural, electronic, magnetic and thermoelectric properties of Zr_2RhAl. *Phys. B Condens. Matter* **552**, 227–235 (2019).

45. Maekawa, T., Kurosaki, K. & Yamanaka, S. Thermal and mechanical properties of perovskite-type barium hafnate. *J. Alloys Compd.* **407**, 44–48 (2006).

46. Yamanaka, S. *et al.* Thermophysical properties of $BaZrO_3$ and $BaCeO_3$. *J. Alloys Compd.* **359**, 109–113 (2003).

47. Kurosaki, K., Konings, R. J. M., Wastin, F. & Yamanaka, S. The low-temperature heat capacity and entropy of $SrZrO_3$ and $BaZrO_3$. *J. Alloys Compd.* **424**, 1–3 (2006).

48. Stenstrop, G. & Engell, J. $BaZrO_3$: Synthesis, Properties and Compatibility with $Ba_2YCu_3O_{7-x}$. *J. Less-Common Metah,* **164**, 200–207 (1990).

49. Azad, A.-M. & Subramaniam, S. Synthesis of $BaZrO_3$ by a solid-state reaction technique using nitrate precursors. *Mater. Res. Bull.* **37**, 85 (2002).

50. Yamanaka, S. *et al.* Heat capacities and thermal conductivities of perovskite type $BaZrO_3$ and $BaCeO_3$. *J. Alloys Compd.* **359**, 1–4 (2003).

51. Moreira, M. L., Andrés, J., Varela, J. A. & Longo, E. Synthesis of fine micro-sized $BaZrO_3$ powders based on a decaoctahedron shape by the microwave-assisted hydrothermal method. *Cryst. Growth Des.* **9**, 833–839 (2009).

52. Gallucci, K., Villa, P., Groppi, G., Usberti, N. & Marra, G. Catalytic combustion of methane on $BaZr_{(1-x)}Me_xO_3$ perovskites synthesised by a modified citrate method. *Catal. Today* **197**, 236–242 (2012).

53. Terki, R., Feraoun, H., Bertrand, G. & Aourag, H. Full potential calculation of structural, elastic and electronic properties of $BaZrO_3$ and $SrZrO_3$. *Phys. status solidi* **242**, 1054–1062 (2005).

54. Sundell, P. G., Björketun, M. E. & Wahnström, G. Thermodynamics of doping and vacancy formation in $BaZrO_3$ perovskite oxide from density functional calculations. *Phys. Rev. B - Condens. Matter Mater. Phys.* **73**, 104112 (2006).

55. Sahoo, M. P. K., Zhang, Y. & Wang, J. Enhancement of ferroelectric polarization in layered $BaZrO_3$/$BaTiO_3$ superlattices. *Phys. Lett. A* **380**, 299–303 (2016).

56. López Garciá, A. R., de la Presa, P. & Rodríguez, A. M. Temperature dependence of the hyperfine interaction in the cubic phase of $BaHfO_3$. *Phys. Rev. B* **44**, 9708–9710 (1991).

57. Alonso, R. E., Horowitz, C., López García, A., Lamas, D. G. & Caneiro, A. Second order tetragonal-to-cubic phase transition in $Sr_{0.5}Ba_{0.5}HfO_3$. *Solid State Commun.* **120**, 205–210 (2001).

58. Li, L., Kennedy, B. J., Kubota, Y., Kato, K. & Garrett, R. F. Structures and phase transitions in $Sr_{1-x}Ba_xHfO_3$ perovskites. *J. Mater. Chem.* **14**, 263–273 (2004).

59. Feteira, A., Sinclair, D. C., Rajab, K. Z. & Lanagan, M. T. Crystal structure and microwave dielectric properties of alkaline-earth hafnates, $AHfO_3$(A=Ba, Sr, Ca). in *Journal of the American Ceramic Society* 91 893–901 (Blackwell Publishing Inc., 2008).

60. Yu, X., Chen, G.-F., Shen, J., Li, Y.-X. & Luo, X.-G. First principle calculation of structural, elastic and electronic properties of $XHfO_3$(X=Ba, Sr). *Acta Phys. Sin.* **56**, 5366–5370 (2007).

61. Liu, Q. J., Liu, Z. T., Feng, L. P. & Tian, H. Mechanical, electronic, chemical bonding and optical properties of cubic $BaHfO_3$: First-principles calculations. *Phys. B Condens. Matter* **405**, 4032–4039 (2010).

62. Azahaf, C., Zaari, H., Abbassi, A., Ez-Zahraouy, H. & Benyoussef, A. Theoretical investigation of spontaneous polarization, electronic and optical properties of cubic perovskite $BaHfO_3$. *Opt. Quantum Electron.* **47**, 2889–2897 (2015).

63. Yangthaisong, A. Electronic and lattice vibrational properties of cubic $BaHfO_3$ from first principles calculations. *Phys. Lett. Sect. A Gen. At. Solid State Phys.* **377**, 927–931 (2013).

64. Robertson, J. Band offsets of wide-band-gap oxides and implications for future electronic devices. *J. Vac. Sci. Technol. B Microelectron. Nanom. Struct.* **18**, 1785–1791 (2000).

Table caption

Table1: Lattice constant α(Å), bulk modulus B(GPa), for the perovskites $BaZrO_3$ and $BaHfO_3$.

Compound	α(Å)	B(GPa)	Method
$BaZrO_3$	4.234	149.8	This work
	4.189[5], 4.193[48], 4.19[6,7,49], 4.192[4,46,50],	103[46,50], 155.9[8],	Exp
	4.2269[8], 4.2063[51], 4.1812[21], 4.1815[52], 4.193[26]	127[11]	
	4.154[7],4.207[53], 4.148[17], 4.25[54], 4.193[11],	175.3[7],157, 174.7[17],	Theory
	4.16[23,55], 4.19[2], 4.198[10]	141[11], 172[2], 168[10]	
$BaHfO_3$	4.212	156.0	This work
	4.171[4,6,45], 4.17[56], 4.172[57], 4.1668[58], 4.1796[59],		Exp
	4.171[11], 4.19[2], 4.193[10], 4.310[60], 4.2499[9],	144[11], 175[2], 171[10],	Theory
	4.170[18], 4.286[12], 4.248[61], 4.160[62], 4.064[63]	123.6[60], 186[9a], 194[9b],	
		146.72[12a], 145.50[12b],	
		179[63]	

[9a, 12a] Obtained from the Voigt–Reuss–Hill (VRH) approximation.

[9b, 12b] Obtained from fitting the third-order Birch–Murnaghan equation

Table 2: The calculated bandgap (Eg) using PBE-GGA and TB-mBJ methods with comparison with previous computational and experimental results

$BaZrO_3$			$BaHfO_3$		
E_g (eV)	method	Ref.	E_g (eV)	method	Ref.
4.42	TB-mBJ	This work	5.25	TB-mBJ	This work
3.39	PBE-GGA	This work	3.69	PBE-GGA	This work
5.3	Exp	[64]	6	Exp (predicted)	[18]
3.9	LDA	[17]	2.99	LDA	[9]
3.156	GGA	[8]	3.94	SX-LDA	[12]
5.4	LCAO	[10]	3.17	GGA	[12]
3.55	Exp.	[21]	5.3	SX-LDA	[63]
4.96	Exp.	[25]	3.9	GGA-PBE	[62]
			5.9	TB-mBJ	[62]

Figure Captions:

Figure 1: Crystal structures of $BaTMO_3$ (TM: blue, Ba: green and O: red).
Figure 2: Band structure of cubic perovskite: a) $BaZrO_3$ PBE-GGA, b) $BaZrO_3$ TB-mBJ, c) $BaHfO_3$ PBE-GGA, and b) $BaHfO_3$ TB-mBJ methods.
Figure 3: Calculated total and Partial-projected DOS: a) $BaZrO_3$ using PBE-GGA compared with TB-mBJ and b) $BaHfO_3$ using PBE-GGA compared with TB-mBJ method.
Figure 4: Calculated optical properties for the $BaHfO_3$ and $BaZrO_3$ compounds, a) $\varepsilon_2(\omega)$, b) $\varepsilon_1(\omega)$, c) α(ω), d) L(ω), e) R(ω), f) n(ω), and g) σ(ω).
Figure 5: Transition coefficients as a function of temperature at ground state chemical potential for the $BaHfO_3$ and $BaZrO_3$ compounds: a) Seebeck coefficient (S), b) electric conductivity rate (σ/τ), c) electronic thermal conductivity (κ^0), d) The power factor (PF).
Figure 6: Seebeck coefficient S as a function of chemical potential at different temperature for a) $BaHfO_3$ and b) $BaZrO_3$.
Figure 7: (a) and (b) are the electrical conductivity rate (σ/τ) as a function of chemical potential at different temperature for both $BaHfO_3$ and $BaZrO_3$; (c) and (d) are the electronic thermal conductivity as a function of chemical potential at different temperature for both compounds $BaHfO_3$ and $BaZrO_3$, respectively.
Figure 8: The power factor ($PF = S^2\sigma/\tau$) as a function of chemical potential at different temperature range for a) $BaHfO_3$ and b) $BaZrO_3$.
Figure 9: The electronic specific heat as a function of chemical potential at different temperature for a) $BaHfO_3$ and b) $BaZrO_3$.
Figure10: The density of state at Fermi level DOS [E_F] as a function of chemical potential at different temperature for a) $BaHfO_3$ and b) $BaZrO_3$.

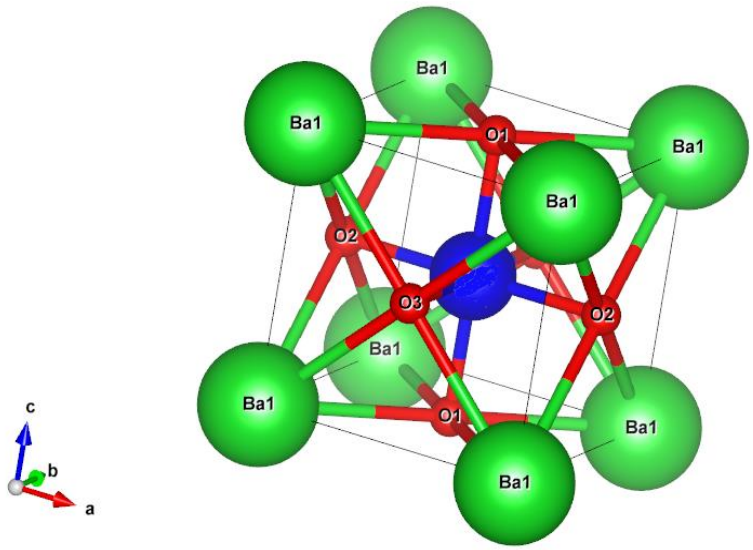

Figure1

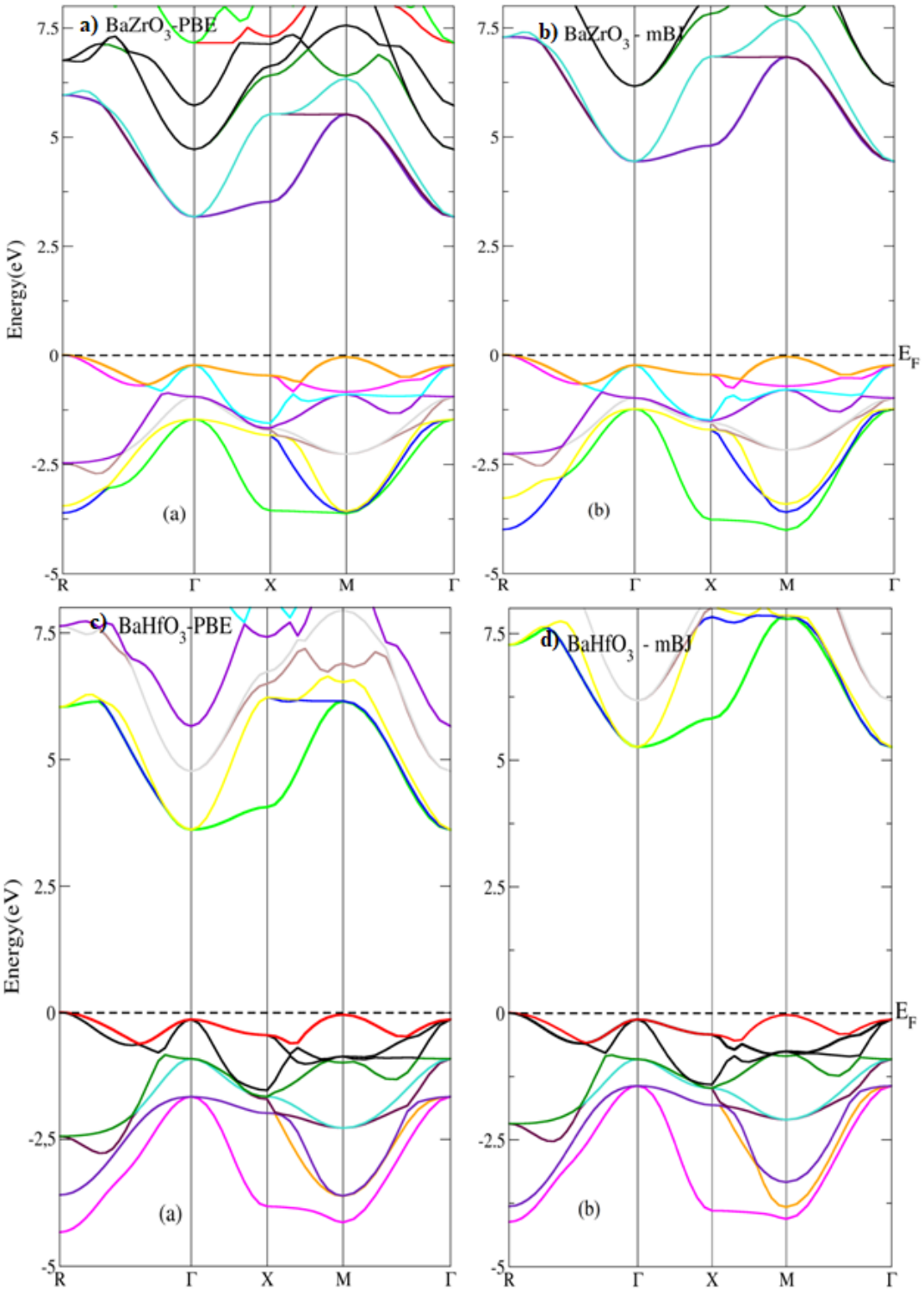
a) BaZrO3-PBE
b) BaZrO3 - mBJ
c) BaHfO3-PBE
d) BaHfO3 - mBJ
Energy(eV)
7.5
5
2.5
0
-2.5
-5
R
Γ
X
M
Γ
E_F
(a)
(b)

Figure 2

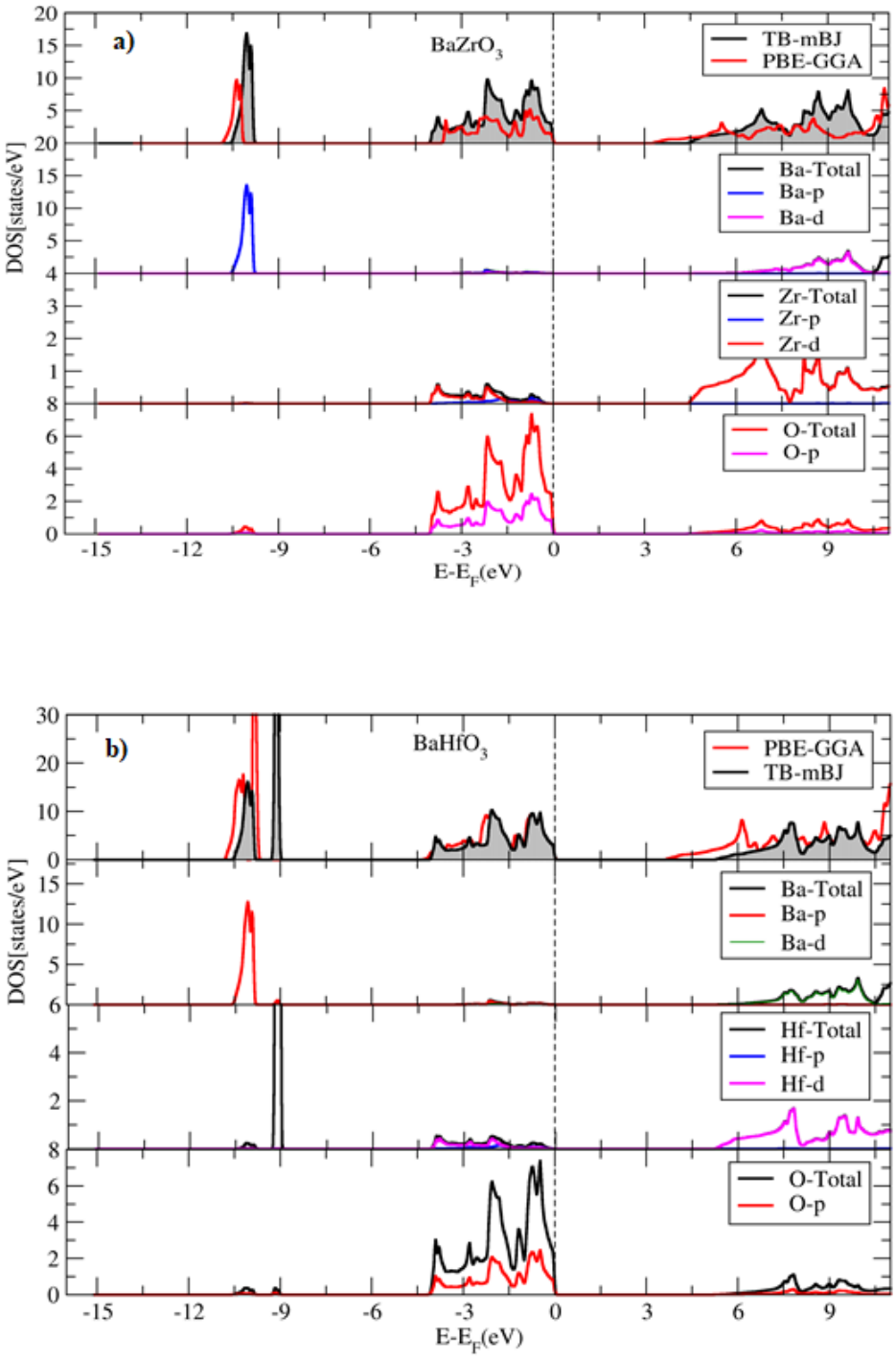
a)
BaZrO3
TB-mBJ
PBE-GGA
Ba-Total
Ba-p
Ba-d
Zr-Total
Zr-p
Zr-d
O-Total
O-p
DOS[states/eV]
E-EF(eV)
b)
BaHfO3
PBE-GGA
TB-mBJ
Ba-Total
Ba-p
Ba-d
Hf-Total
Hf-p
Hf-d
O-Total
O-p
DOS[states/eV]
E-EF(eV)

Figure3

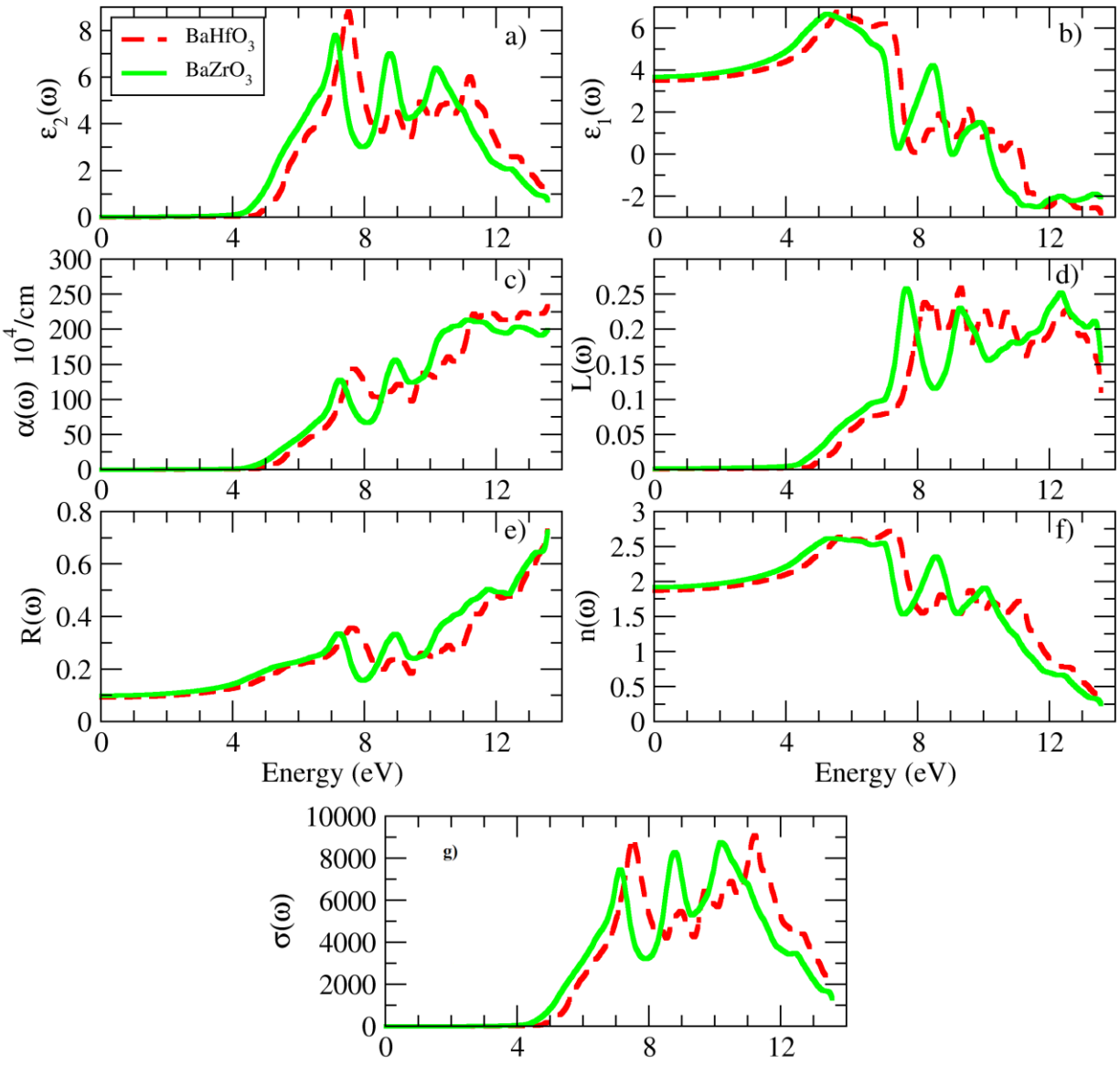
BaHfO3
BaZrO3
a)
b)
c)
d)
e)
f)
g)
ε2(ω)
ε1(ω)
α(ω) 10^4/cm
L(ω)
R(ω)
n(ω)
σ(ω)
Energy (eV)
Energy (eV)

Figure 4

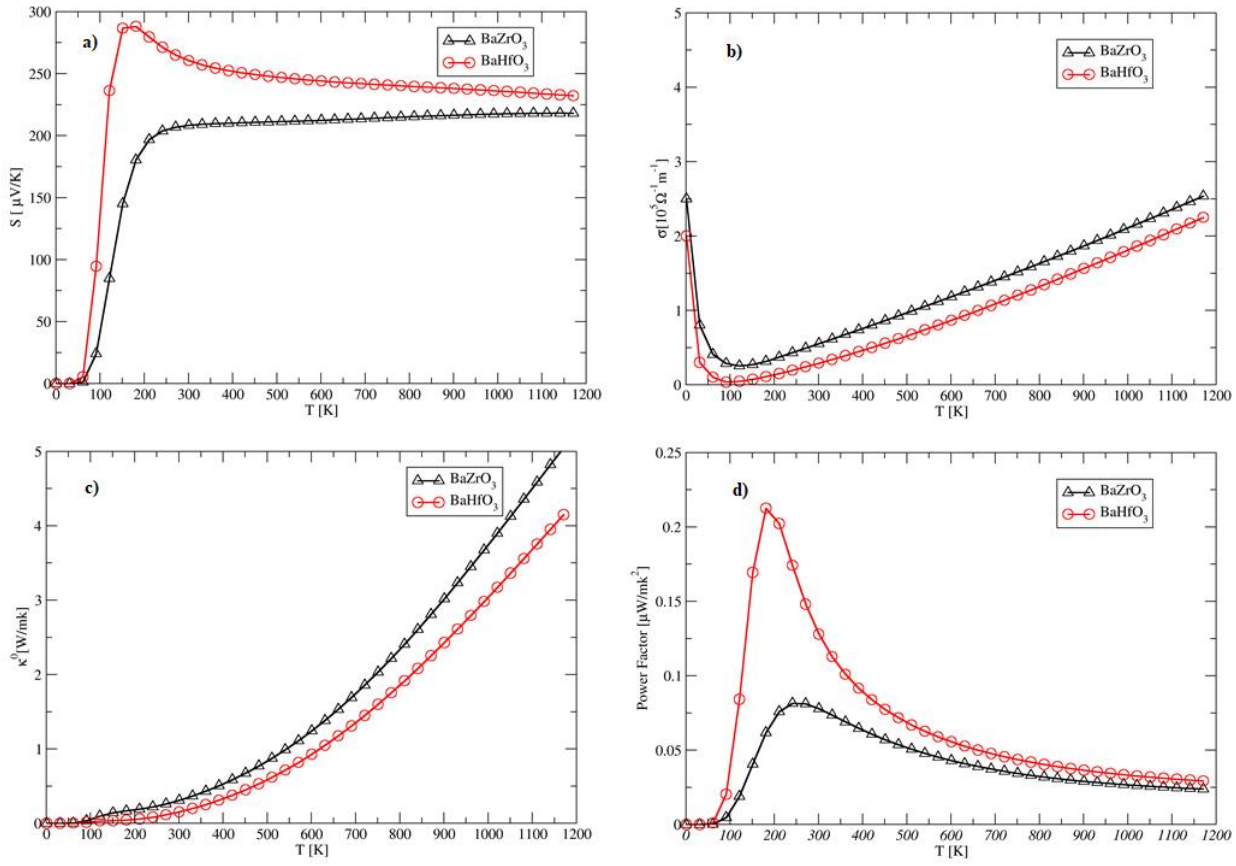
a)
BaZrO3
BaHfO3
S [μV/K]
T [K]
b)
BaZrO3
BaHfO3
σ[10^5 Ω^-1 m^-1]
T [K]
c)
BaZrO3
BaHfO3
κ^0 [W/mk]
T [K]
d)
BaZrO3
BaHfO3
Power Factor [μW/mk^2]
T [K]

Figure 5

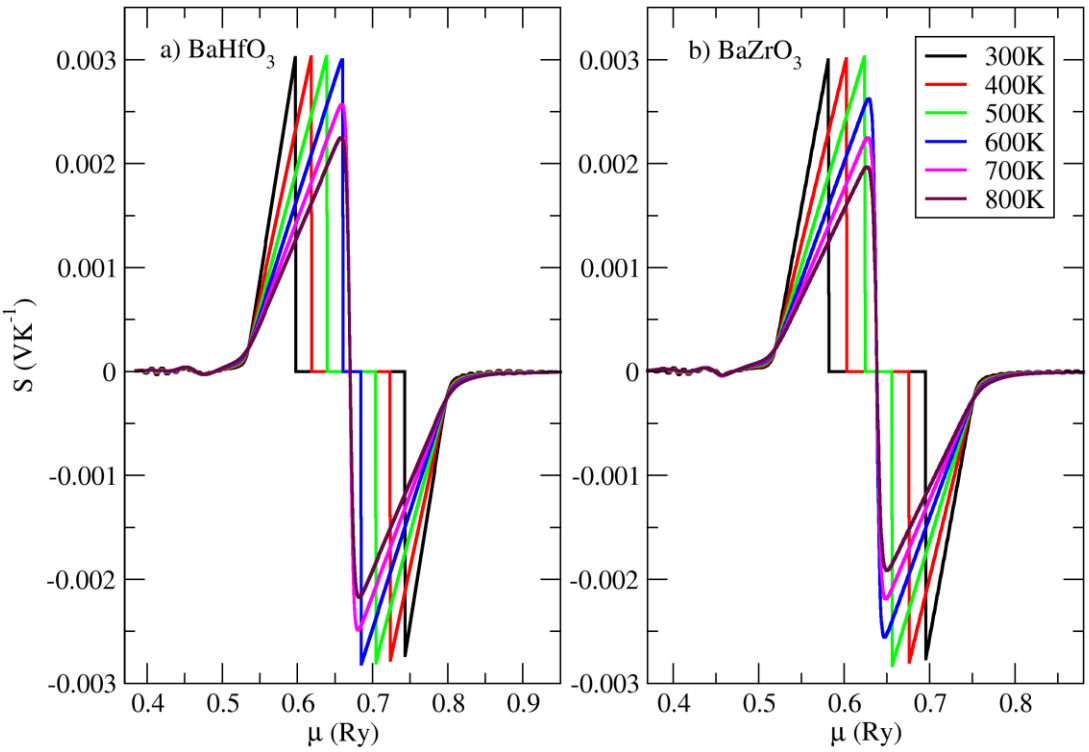
a) BaHfO3
b) BaZrO3
300K
400K
500K
600K
700K
800K
S (VK-1)
μ (Ry)
0.003
0.002
0.001
0
-0.001
-0.002
-0.003
0.4
0.5
0.6
0.7
0.8
0.9

Figure 6

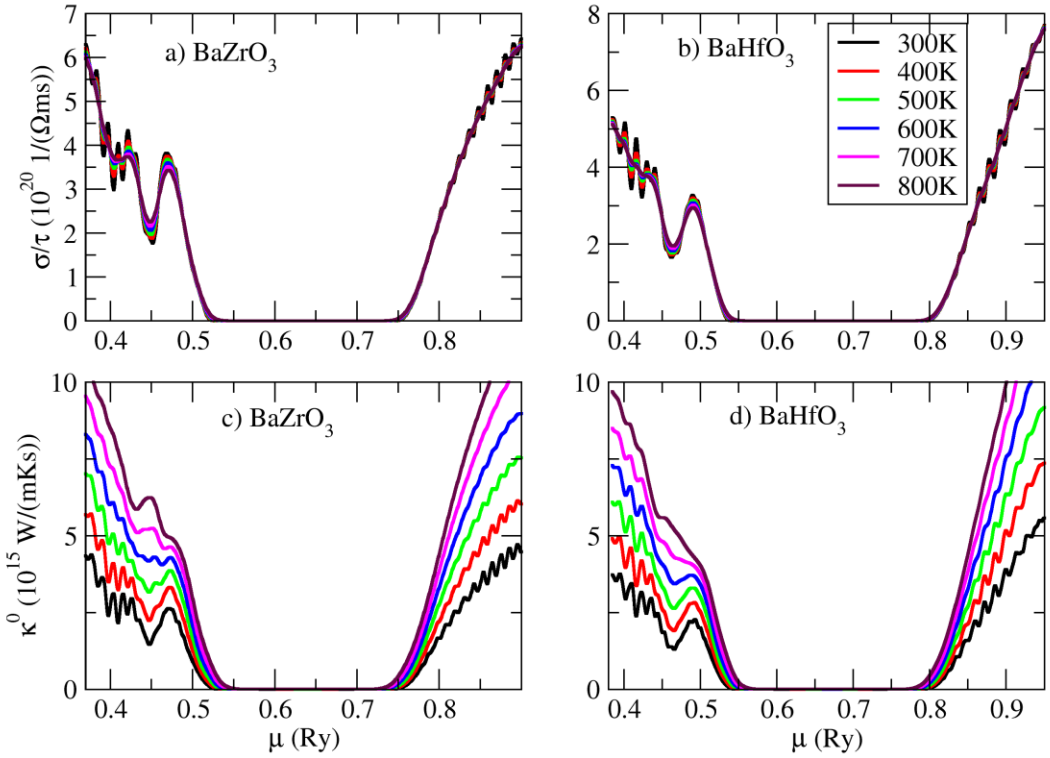
a) BaZrO3
b) BaHfO3
c) BaZrO3
d) BaHfO3
300K
400K
500K
600K
700K
800K
σ/τ (10^20 1/(Ωms))
κ0 (10^15 W/(mKs))
μ (Ry)
μ (Ry)

Figure 7

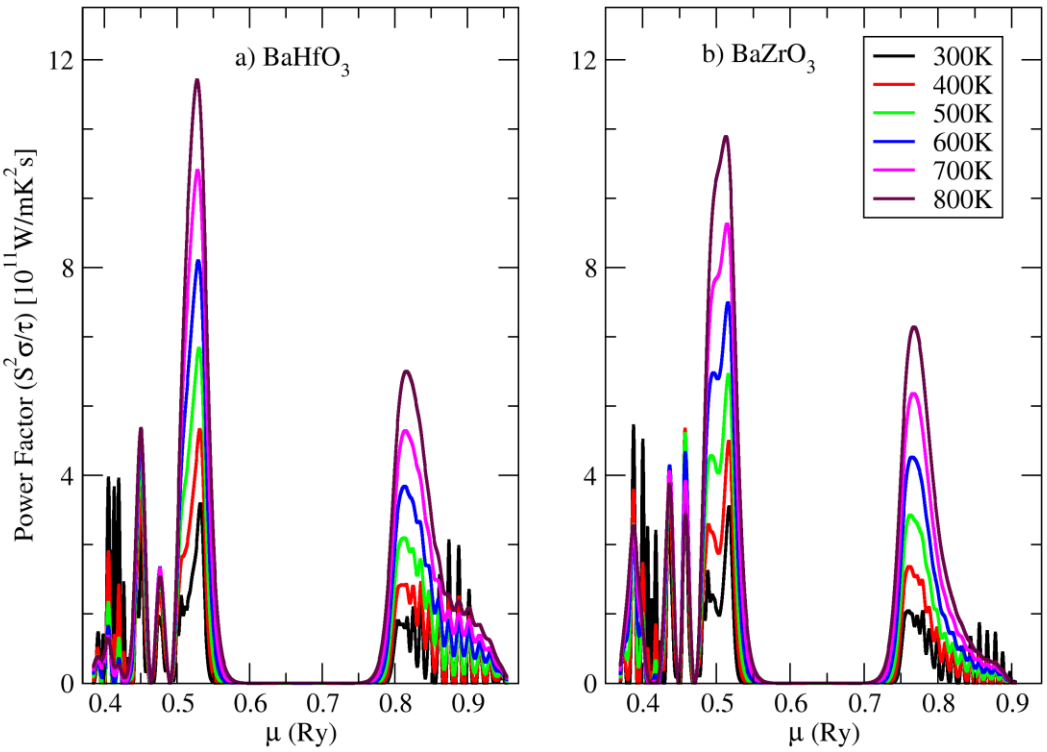
a) BaHfO3
b) BaZrO3
300K
400K
500K
600K
700K
800K
Power Factor (S2σ/τ) [10^11 W/mK2s]
μ (Ry)
μ (Ry)
0
4
8
12
0.4
0.5
0.6
0.7
0.8
0.9

Figure 8

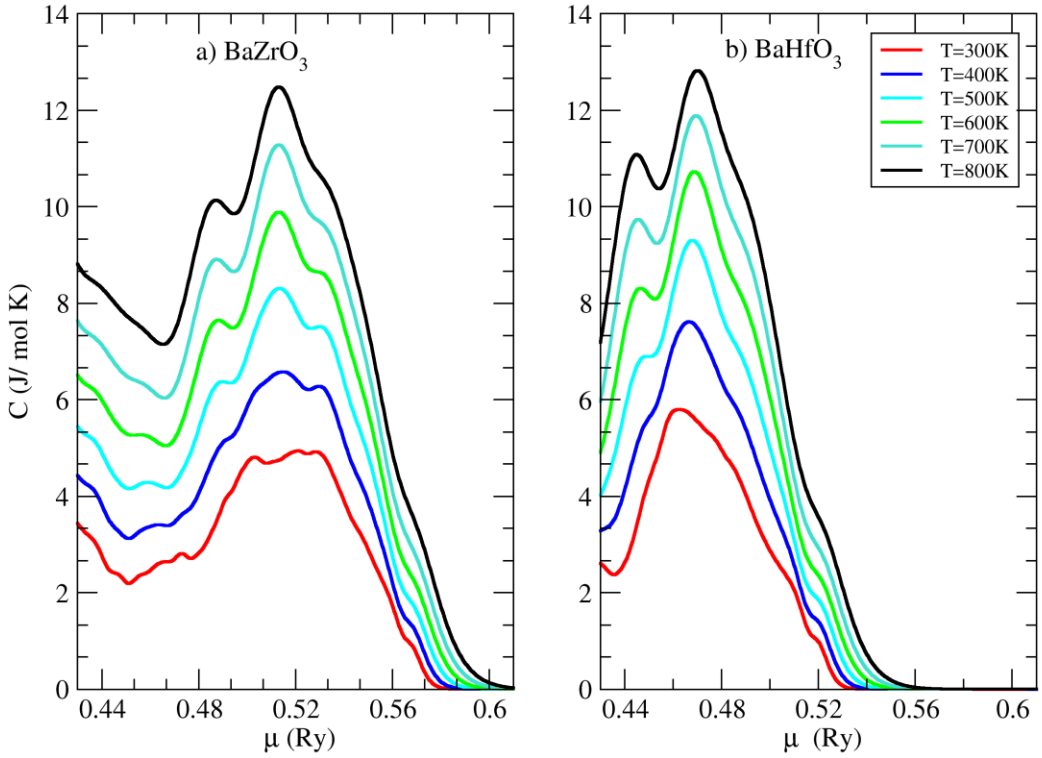
a) BaZrO3
b) BaHfO3
T=300K
T=400K
T=500K
T=600K
T=700K
T=800K
C (J/ mol K)
μ (Ry)
μ (Ry)
0
2
4
6
8
10
12
14
0.44
0.48
0.52
0.56
0.6

Figure 9

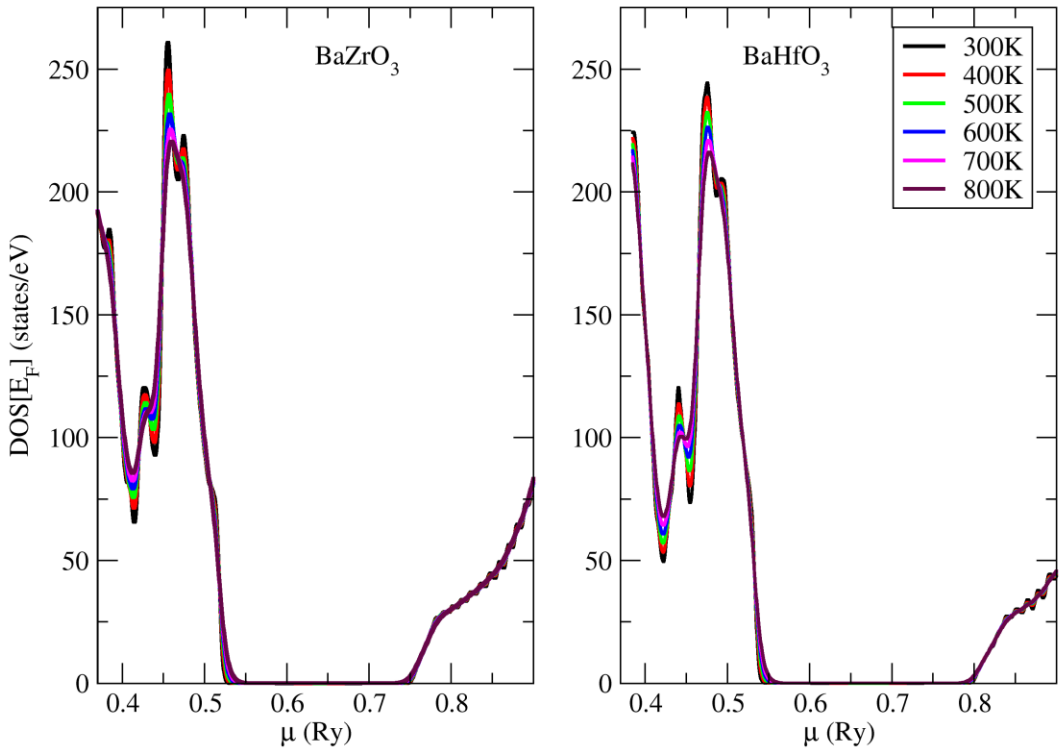
BaZrO3
BaHfO3
300K
400K
500K
600K
700K
800K
DOS[EF] (states/eV)
μ (Ry)
μ (Ry)
0
50
100
150
200
250
0.4
0.5
0.6
0.7
0.8

Figure 10